



Schweizerische Eidgenossenschaft
Confédération suisse
Confederazione Svizzera
Confederaziun svizra

Eidgenössisches Departement des Innern EDI
Bundesamt für Meteorologie und Klimatologie MeteoSchweiz

Arbeitsbericht MeteoSchweiz Nr. 238

Automatic Hail Detection at MeteoSwiss

Verification of the radar-based hail detection algorithms POH, MESHS and HAIL

M. Betschart, A. Hering



Arbeitsbericht MeteoSchweiz Nr. 238

Automatic Hail Detection at MeteoSwiss

Verification of the radar-based hail detection algorithms POH, MESHS and HAIL

M. Betschart, A. Hering

Bitte zitieren Sie diesen Arbeitsbericht folgendermassen

Betschart, M., Hering, A.: 2012, Automatic Hail Detection at MeteoSwiss – Verification of the radar-based hail detection algorithms POH, MESHS and HAIL, *Arbeitsberichte der MeteoSchweiz*, **238**, 59 pp.

Herausgeber

Bundesamt für Meteorologie und Klimatologie, MeteoSchweiz, © 2012

MeteoSchweiz
Krähbühlstrasse 58
CH-8044 Zürich
T +41 44 256 91 11
www.meteoschweiz.ch

Weitere Standorte
CH-8058 Zürich-Flughafen
CH-6605 Locarno Monti
CH-1211 Genève 2
CH-1530 Payerne

I. Abstract

MeteoSwiss operates a network of three different radar stations. The radar-based hail detection algorithms POH (Probability Of Hail), MESHS (Maximum Expected Severe Hail Size) and HAIL were verified in this study. The years 2009, 2010 and 2011 were considered. A ground-truth hail report data base was created. Data for the year 2011 were collected in Internet with information about locations and hailstone diameters. For the years 2009 and 2010 insurance data were used. In total 11984 single hail reports were available. Merged at municipal level 3644 reports were used. Ground-truth hail observations and radar-based hail products were visualized in Google Earth. A 3x3 verification matrix was used for the verification process. Scoring parameters were calculated. An overall CSI (Critical Success Index) of POH of 0.79 was found with POD (Probability Of Detection) of 0.97 and FAR (False Alarm Rate) of 0.19. For the MESHS algorithm an overall CSI of 0.79 was calculated with a corresponding POD value of 0.83 and FAR value of 0.06. The biases showed that POH overestimates the occurrence of hail, while MESHS underestimates the hail areas. PODs were calculated from a point-based perspective while FARs were computed from a hail swath-based perspective. For the hail detection algorithm HAIL an overall POD of 0.84 was found. Correlations between the MESHS algorithm and the maximum observed hail size diameters of 2011 were low. The analysis of POH emphasized that lower probabilities of hail were detected for hailstone diameters smaller than 2.5 cm.

II. Table of Contents

I. ABSTRACT	II
II. TABLE OF CONTENTS.....	IVV
1. INTRODUCTION, OBJECTIVES.....	1
1.1. INTRODUCTION	1
1.2. MOTIVATION, OBJECTIVES	3
2. GENERAL ASPECTS.....	5
2.1. HAIL	5
2.1.1. <i>Definition of hail</i>	5
2.2. RADAR.....	6
2.2.1. <i>Swiss radar network</i>	6
2.2.2. <i>Hail detection products</i>	6
2.2.2.1. POH.....	6
2.2.2.2. MESHS.....	8
2.2.2.3. HAIL	9
3. METHODS	10
3.1. COLLECTION OF HAIL VERIFICATION DATA	10
3.1.1. <i>Sources</i>	10
3.1.2. <i>Information about location</i>	12
3.1.3. <i>Information about hail diameter</i>	12
3.1.4. <i>Data 2009/2010</i>	13
3.1.5. <i>Data 2011</i>	13
3.2. RADAR DATA	14
3.2.1. <i>Radar-based hail data 2011</i>	15
3.2.2. <i>Radar-based hail data 2009/2010</i>	15
3.2.2.1. <i>Recalculation of POH and MESHS outputs for 2009/2010</i>	15
3.3. VISUALIZATION	15
3.3.1. <i>Georeferencing observations</i>	17
3.3.2. <i>Georeferencing of radar images</i>	20
3.3.3. <i>Adaption of radar images for Google Earth</i>	21
3.3.4. <i>KML-file for Google Earth</i>	23
3.3.5. <i>Kmz-file for Google Earth</i>	23
3.3.6. <i>Animation POH and MESHS in Google Earth</i>	24
3.4. 3X3 VERIFICATION MATRIX	25
3.5. VERIFICATION SCORES	28
3.5.1. <i>Contingency table</i>	28
3.5.2. <i>Probability of Detection</i>	28
3.5.3. <i>False Alarm Rate</i>	29
3.5.4. <i>Critical success index</i>	33
3.5.5. <i>Bias</i>	33
3.5.6. <i>Goodness of MESHS</i>	34
4. RESULTS	35
4.1. VERIFICATION SCORES	35
4.1.1. <i>Verification scores 2009</i>	35
4.1.2. <i>Verification scores 2010</i>	36
4.1.3. <i>Verification scores 2011</i>	37
4.1.4. <i>Overall verification scores</i>	37
4.2. MESHS	39

4.3.	POH.....	41
4.4.	CLIMATOLOGY.....	41
4.4.1	<i>Radar-based hail climatology</i>	43
4.5.	POH 4TH GENERATION	45
5.	CONCLUSION AND RECOMMENDATIONS	46
6.	ACKNOWLEDGEMENTS.....	48
7.	APPENDIX.....	49
7.1.	<i>Correlation MESHs</i>	50
7.2.	<i>Calculations FAR 2009/2010</i>	51
7.3.	<i>Radar based hail climatology</i>	53
7.4.	<i>Examples of well captured small scale hail events</i>	57
8.	REFERENCES.....	58

1. Introduction, objectives

1.1 . Introduction

Weather radar detect different kinds of hydrometeors such as rain, snow and hail. Several hail detection algorithms have been developed (e.g. Waldvogel et al., 1979; Treloar, 1998; Witt et al., 1998). Today, radar-based hail detection algorithms are widely used and deliver different types of information about hail. On the one hand, there exist probabilistic hail detection algorithms (e.g. Waldvogel et al., 1979). On the other hand, hail detection algorithms which are able to give information about the hail size are widely in use (e.g. Treloar, 1998; Witt et al., 1998).

Several hail verification studies have been realized (e.g. Kessinger et al., 1995; Witt et al., 1998; Schiesser et al., 1998; Holleman, 2001; Ortega et al., 2006; Ortega et al., 2009; Wilson et al., 2009; Hyvärinen et al., 2010). The difficulty in realizing verifications of hail detection algorithms is the insufficient volume of ground-truth data. In order to verify radar-based hail algorithms, ground-based hail observations have to be available in a sufficient and accurate temporal and spatial resolution. According to Kessinger's study, in total 237 different hail reports of 97 hailstorms have been used. Witt et al. (1998) verified the hail detection algorithm (HAD) for the WSR-88D weather surveillance radar system, which is based on Waldvogel's method. For this purpose, they used 107 different ground-truth hail observations of 10 different days from *Storm Data*. In order to verify eight different hail detection products, Holleman (2001) used hail observations by synop stations and precipitation stations, reports of hail damage from three agricultural insurance companies, reports by weather amateurs, and newspapers. Ortega et al. (2006) used data of SHAVE (Severe Hail Verification Experiment). Four different hail fall cases were verified, and the evolution of hailstone diameters was studied. The Internet is another source of weather-related data nowadays. Hyvärinen et al. (2010) used social media such as Flickr¹ to collect ground-truth data about hailstorms in Finland. Ortega et al. (2009) used SHAVE data as well, but for May–August of 2006-2008. Methodological, interviews were used for the project SHAVE. These were collected and then used as source for verifications. In order to gain information about hail and its size, students called persons and companies at certain locations where they expected hail due to radar-based products. Therefore, the SHAVE data set is highly resolved in time and space. Wilson et al. (2009) used SHAVE data for verifications as well. In total 3921 individual reports were used.

The common aim of all radar-based hail algorithm verifications is the classification of hail events in categories of hit and miss events. Authors used different tolerances to make the determination whether ground-truth hail observations were hit or missed by the radar products. Kessinger et al. (1995) used spatial tolerances up to 15 km and temporal tolerances of 6 minutes. Witt et al. (1998) used spatial tolerances up to 30 km. A ground-truth observation was counted as hit within a temporal

¹ www.flickr.com

tolerance up to 60 minutes. The positioning tolerance of Holleman (2001) was 12.5 km. The temporal resolution was 24 hours. Hyvärinen et al. (2010) used spatial tolerances of 2 km and temporal tolerances of about 15 min in order to georeference their ground-truth data. The verification itself was a rough synchronization with the radar images. In the study by Ortega et al. (2009) a spatial tolerance of several kilometers was accepted and the temporal resolution was 60 minutes. Wilson et al. (2009) applied a point-by-point analysis to compare maximum expected hail size (MESH) values with SHAVE reports.

In comparing different verification results with each other, note that the results themselves depend strongly on defined spatial and temporal tolerances. The evaluation of the performances of radar-based hail detection algorithms is difficult due to the lack of available ground-truth verification data (Witt et al., 1998). Scoring parameters, such as POD (probability of detection), FAR (false alarm rate) and CSI (critical success index), are widely in use (Donaldson et al., 1975; Wilks, 1995). Kessinger et al. (1995) found values of 79 % probability of detection (POD) and false alarm rate of 17 % (FAR) for a POH product with hail threshold ≥ 6 mm. (NHailPH). High variability was found for HDA by Witt et al. (1998) with an overall POD of 78 % and an overall FAR of 69 %. CSI values up to 54 % with POD around 65 % and FAR 20 % were found by Holleman (2001) for a POH algorithm based on Waldvogel's method and a warning threshold of 1.75 km for the year 1999. Ortega et al. (2006) hints that the use of MESH (maximum expected size of hail) are not suited characterizing the size of the hail fall, as other cases had similar MESH and low level reflectivity with much larger hail. Three years later, more extensive SHAVE data showed a wide range of hail size for a given MESH (Wilson et al. 2009). Further, they found that MESH usually overestimates the maximum size of hail that will reach the earth's surface. The spread of reported hail sizes that correspond to each MESH value was large. For MESH with a threshold of 19 mm POD of 80% and FAR of 50 % were found.

Scientists have started to use Google Earth² as background map in order to visualize radar-based imagery. A variety of multi-sensor severe weather products are generated by NSSL (National Severe Storm Laboratory), and shared to Google Earth (Smith et al., 2006). Radar-based hail swath images have been overlaid during the SHAVE experiment (Smith et al., 2006; Ortega et al., 2006, 2007, 2009; Wilson et al., 2009). Ground-truth hail data, collected during the SHAVE experiment, were visualized in Google Earth as well. This approach compares hail swaths, generated due to hail-detection algorithms, with ground-truth observations. The simple handling of Google Earth makes it possible to plot radar data in short time intervals. Therefore, this information is extremely valuable to emergency management officials in a disaster response situation (Smith et al., 2006). Ortega et al. (2006, 2009) and Wilson et al. (2009) used Google Earth in order to verify hail detection algorithms.

² www.earth.google.com

1.2 . Motivation, objectives

Weather radar and its applications have a long history in Switzerland. Today, MeteoSwiss operate a network of three radar stations in Switzerland. The locations are Albis near Zurich, La Dôle near Geneva and Monte Lema in Ticino. The main task of the radar network is monitoring and warning of dangers due to different weather phenomena such as heavy precipitation, snowfall and hail. Severe hail mostly occurs during the summer season, when thunderstorm activities are the most intense. Hail events mostly occur very local (OcCC, 2003). Past experience has shown that severe hailstorms can cause substantial damage and significant losses to insured property, especially if hailstorms move over densely populated areas (Hohl et al., 2002). Switzerland with its 238 inhabitants per square kilometer (Swiss Federal Statistical Office, 2000) is one of the densest populated countries. Note that this aspect is even more important due to the circumstance that nearly all people live in the Swiss plateau, which accounts for 30 % of Switzerland's area. In order to detect hailstorms, different methods using single-polarization radar have been developed. MeteoSwiss operate three hail detection algorithms in real time. The first, simplest and oldest of them is HAIL, which distinguishes between two categories, possible hail and probable hail, for hailstorms. The second product which is able to detect hail is called POH (Probability Of Hail) and gives an estimation of the probability of hailstorm for a certain location in Switzerland. The third product is called MESHS and is an acronym for Maximum Expected Severe Hail Size. As the name implies, this product calculates the expected severe hail size for a certain area in Switzerland (Hering, 2010).

Radar meteorologists have been looking for precise hail detection algorithms since the beginnings of radar research. Holleman et al. (2001) found that methods for the detection of hail in general are more successful than those estimating hail sizes. In order to verify the algorithms of MeteoSwiss, first case studies were made. Those first case studies indicated that the different algorithms work sufficiently in order to detect hail pixels. Unfortunately, a wider study has not been done yet. Holleman et al. (2001) have shown that most hail detection methods have been developed elsewhere, and the methods probably have to be re-tuned to account for differences in the climatological conditions and in the radar systems. Therefore, it is not possible simply to adapt results of other studies. It is necessary to verify the hail detection algorithms of MeteoSwiss by a specific study.

The main goal of this study was to verify the goodness of MeteoSwiss's single-polarized radar hail detection products, HAIL, POH and MESHS. Therefore, a separate ground-based hail observation data base was created. Recent publications have emphasized that internet and social media can be a new source for weather-related data (Hyvärinen et al., 2010). The verification referred on the years 2009, 2010 and 2011. Hailstorms mostly occur from May-September. These months only were considered. For 2009 and 2010, insurance loss data were used to verify the radar detection algorithms. Social media and other internet sources were used for 2011. In contrast to insurance loss data, the hail observations collected on the Internet mostly contained reports about the hail size. Therefore, the social media data were used to verify the detected hail sizes of the MESHS algorithm.

Probability of detection (POD) and false alarm rate (FAR) are important quantities in order to compare the different radar-based hail detection products. Hailstorms are local phenomena and ground-based hail reports are in general very rare. Therefore, it was not possible to achieve a grid-based verification data set. In this study, POD and FAR were determined with a point-by-point analysis, due to the fact that the number of ground-truth reports was much lower than the number of pixels of a radar image. The verification was related to the number of ground-truth reports and not to the number of pixels. This method allows to obtaining reliable results. Google Earth was used to overlay radar data and ground-truth observations. The objectives of this study were as follows:

- Use Internet as source of ground-truth hail data and create a high resolution ground-truth hailstorm data-base for the years 2009, 2010 and 2011;
- recalculate the daily POH and MESHS product of MeteoSwiss for 2009 and 2010 and improve the extent of the archive;
- calculate scoring parameters such as POD, FAR, CSI and bias;
- verify the correlation of MESHS with ground-truth hail observations;
- apply Google Earth as tool in order to visualize radar data and hail swaths;
- enhance climatological information about hail in Switzerland;
- explore first differences of POH fourth generation³.

³ Due to the Swiss radar network renewal, the POH algorithm is adapted in terms of spatial resolution as well as a slight adaption of the algorithm itself.

2. General aspects

2.1. Hail

2.1.1. Definition of hail

Hail is frozen hydrometeors with diameter > 0.5 cm. Holleman (2001) distinguished between summer hail and winter hail. Winter hail mostly occurs when the freezing level is close to the surface and large-scale vertical motion, e.g. due to the passage of a front, forms small hail (≤ 2 cm). Summer hail is defined as larger hail on a small scale, associated to summertime thunderstorms. Large summer hail with its large mass and high terminal velocity can cause severe damage and is potentially dangerous (Holleman, 2001). Table 2.1 shows hail and its terminal velocity as a function of its diameter. Hail smaller than 0.5 cm is called graupel.

Table 2.1: Hail diameter, its terminal velocity (left) and related descriptions (right) after Ludlam (1980), adapted by Holleman (2001).

Kind	Diameter (cm)	Velocity (m/s)	Description
Small	<0.5		Grain
	0.5-1.0		Pea
	1.0-1.5		Mothball; small marble
	1.5-2.0	19	Cherry; marble
Large	2.0-2.5		Large marble
	2.5-3.0	24	Walnut
	3.0-4.0	28	Golfball
	4.0-5.0	31	Small egg
Giant	5.0-6.2	34	Egg
	6.2-7.5	38	Tennis ball

The hail size distribution within a hail cell varies strongly. The same is true for hail stones which can be found on the ground. Hailpad measurements have shown that there is almost ever a huge range in terms of the hail size distribution (Stanley, 1970). One has to be aware of the effect of potential errors while considering human observations of hailstone sizes. Severe hail is defined by convention as hail stone sizes with 2 cm diameter or larger. This threshold is based on the criterion for severe hail in the United States (e.g. Johns et al., 1992). The 1.9-cm (3/4 in.) criterion in the United States came from “the smallest size of hailstones that could cause significant damage to an airplane flying at speeds between 200 and 300 mph [89 and 134 ms^{-1}].”

2.2. Radar

This chapter shortly introduces the basics which are necessary for a better understanding of the following chapters. Further information about the Swiss radar network and its different radar products can be found in the literature (e.g. Joss et al., 1997; Hering et al., 2004; Germann et al., 2006).

2.2.1. Swiss radar network

MeteoSwiss operates a network of three C-band Doppler radar stations. Radar meteorology has a long tradition in Switzerland and especially in Locarno-Monti. The radar network has been including the three radar sites Monte Lema, Albis and La Dôle and is operational with all three radar since 1995. On the basis of life expectancy, all radar will be renewed by 2013 and two new radar will be built, one in canton Valais and the other in canton Grisons. The new generation of dual-polarized Doppler radar will enhance the detection and classification of precipitation, snow and hail considerably. With the two new radar in Valais and Grisons, visibility will also be enhanced due to the altitude of locations and their unconfined scanning range.

For this study only single-polarized data are used. Due to the renewal process of the network, the radar composite was based on two or three radar, depending on the date. The availability of the radar is visible on the radar images. It has to be aware, that not all three radars were available during the time period of this study, especially not during the year 2011. Therefore the detection of weak hail cells was not guaranteed in every situation. It is possible that the radar measurements could miss a weak hail event. This possible lack of hail detection is not further considered in this study.

2.2.2. Hail detection products

The operational single polarization hail detection products POH, MESHS and HAIL were available with 2x2 km spatial resolution and were computed for the composite radar domain. The temporal resolution was 5 minutes for all three products.

2.2.2.1. POH

The POH product shows the grid-based probability of hail for each pixel. The algorithm estimates the probability of hail of any size on the ground (Hering, 2010). The basic criterion of the POH algorithm was introduced by Waldvogel et al. (1979) and is the relation between the 45 dBZ contour height (H_{45}) and the melting level (H_{T0}). Witt et al. (1998) then found a probability of hail as a function of $H_{45} - H_{T0}$. The probability of hail increases with the height difference. Differences greater than 6 km have 100% probability and less than 1.6 km give 0%. For the MeteoSwiss POH product, the zero degree height is

extracted from COSMO-2 model runs. As far as possible, the latest model run is used. Missing values due to the height of the Alps are interpolated for this approach. Figure 2.1 shows an example of the real-time POH product at 14.20 UTC on July 07 2011. At this time, hail with 2 cm diameter measured on the ground.

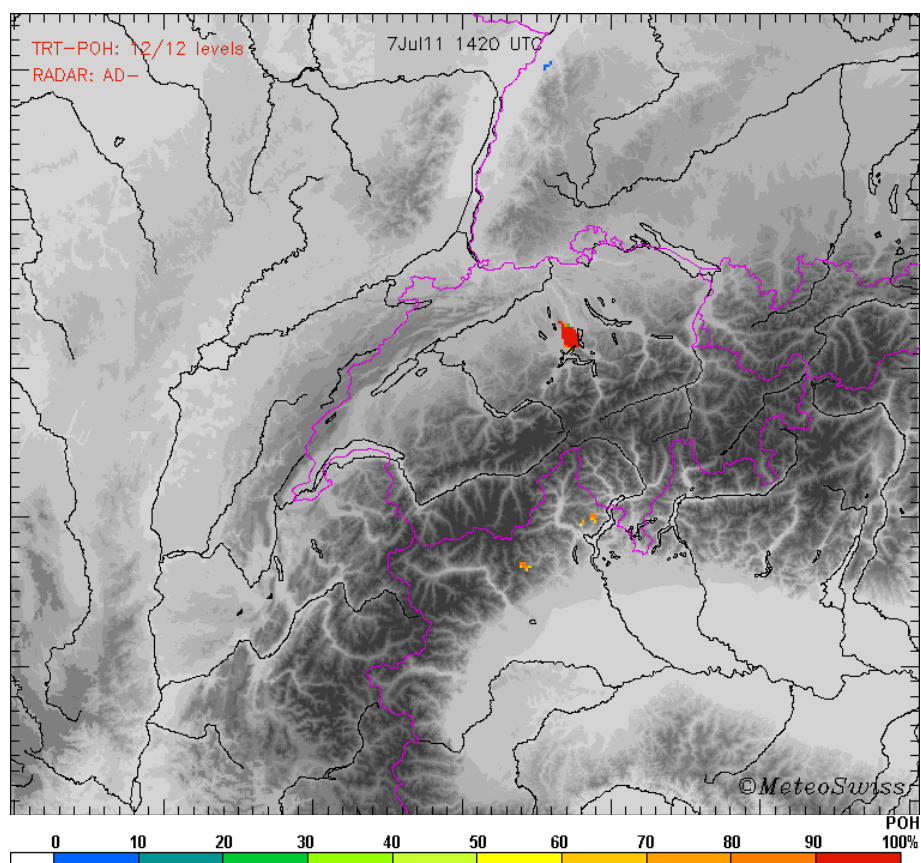


Figure 2.1: POH output at 14.20 UTC on July 7 2011 with hail cell over central Switzerland (red). Red and orange colors mean high probabilities up to 100% whereas green and blue colors present low probabilities between 0 and 50%.

2.2.2.2. MESHS

The Maximum Expected Severe Hail Size (MESHS) is a grid-based estimation of the maximum hail diameter for each pixel within the radar composite. Treloar (1998) developed a heuristic method in order to detect different severe (> 2 cm) hail size diameters, using the difference between the maximum height of the 50 dBZ echo top altitude and the height of the freezing level. For the MeteoSwiss MESHS algorithm, the 51 dBZ height is used due to the specifications of the Swiss radar network. The maximum hail size is represented in 0.5 cm classes. Hail sizes less than 2 cm are not computed. The zero degree height is extracted from the latest COSMO-2 model run. The missing values due to the higher elevation of the Alps are interpolated. Figure 2.2 shows an example of MESHS at 14.30 on July 07 2011.

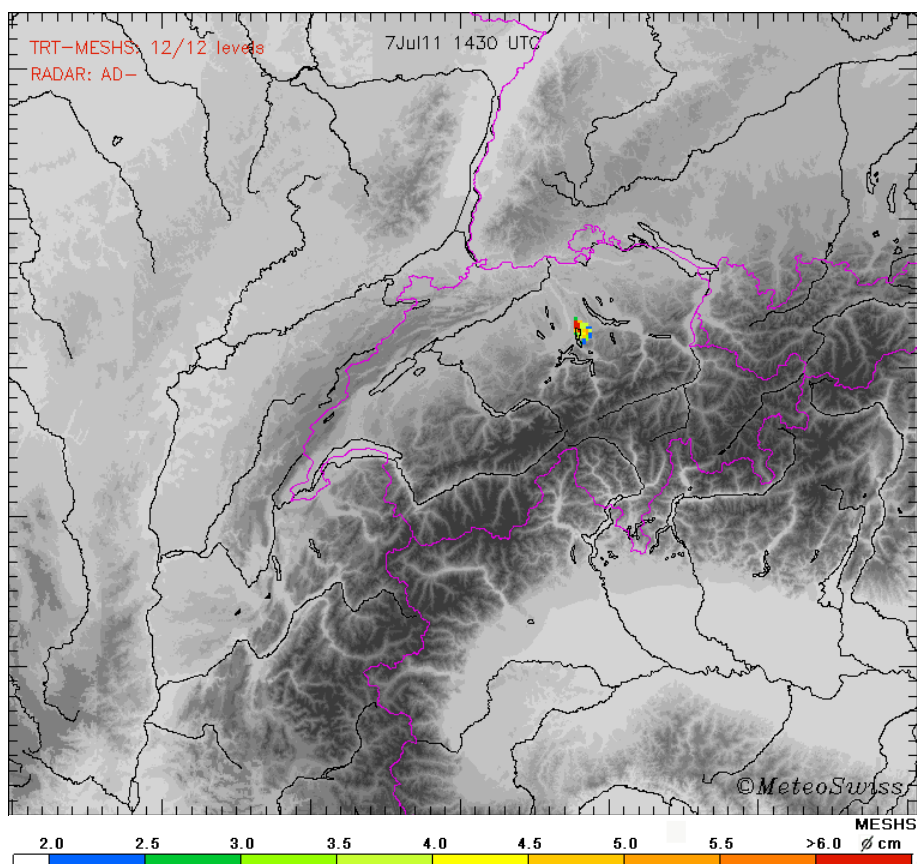


Figure 2.2: MESHS output at 14.30 UTC on July 7 2011.

2.2.2.3. HAIL

The HAIL product is the simplest estimation of the locations of hailstorms. HAIL shows the grid-based estimation of hail. For this product, only the radar reflectivity factor Z is used. Therefore it is possible to distinguish between light rain, possible hail and probable hail. All reflectivities $Z \geq 55$ dBZ are categorized as HAIL probable (red). $Z \geq 52$ dBZ but ≤ 55 dBZ are categorized as HAIL possible (green). Lower Z values are rain. Figure 2.3 shows the integrated HAIL product over 3 hours until 16.35 UTC on July 7 2011. It can easily be recognized that there were several hail tracks from south-west to north-east over the southern part of Ticino.

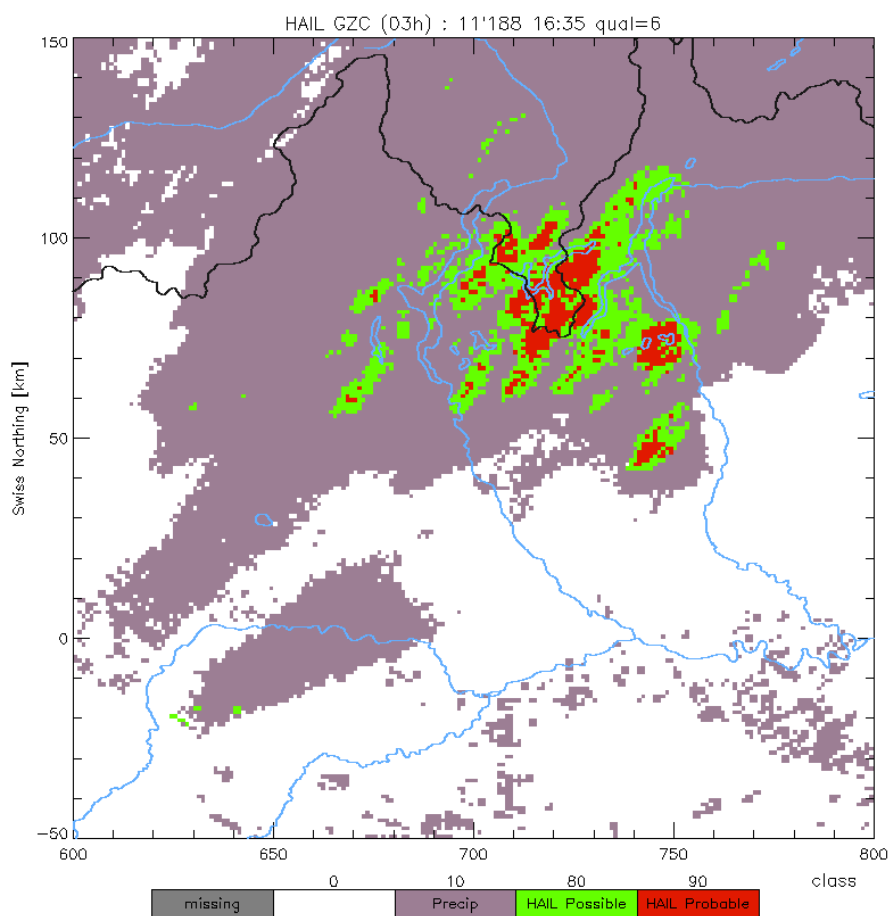


Figure 2.3: Integrated HAIL product over 3 hours until 16.35 UTC on 7 July 2011 over the southern Ticino.

3. Methods

3.1. Collection of hail verification data

One of the major problems in verifying of radar-based hail measurements is that there are not any data about observed hail events available. Obviously, it is less a problem of the amount of radar data available than the amount of real hail observations. Except for first experimental databases, such as the ESWD (European Severe Weather Database) or SYNOP (Surface Synoptic Observations) observations due to manned stations, hardly any information about hailstorms is available. It is not possible to find any complete database about hail events. For this project other sources had to be found.

3.1.1. Sources

In the introduced hail verification studies, different methods were used to detect or measure hail on the ground. Typically used ground-truth data are delivered from:

- *Direct measurements or observations*
 - *SYNOP – Surface Synoptic Observations*
 - *storm reports (Storm Data, USA)*
- *Hailpads*
- *Insurance data*

Nowadays there are other new potential ground-truth data available such as:

- *Internet and social media*

Unfortunately, in Switzerland the more classic data sources cannot be used. No hail measurement network exists and no storm reports are made. Hailpads have to be replaced regularly and are therefore time consuming and expensive to operate. In Switzerland no hail pad network exists and therefore no hail pad data are available.

For this study two ground-truth hail data sources were available. First, loss data were used from the Swiss hail insurance⁴ and the Lucerne building insurance⁵ for the years 2009 (SHVDB09⁶) and 2010 (SHVDB10⁷). Second, the Internet was used in order to collect ground-truth data for the year 2011 (SHVDB11⁸).

⁴ Schweizer Hagel; <http://www.hagel.ch>

⁵<http://www.gvl.ch>

⁶ Swiss Hail Verification Data Base 2009

⁷ Swiss Hail Verification Data Base 2010

⁸ Swiss Hail Verification Data Base 2011

In total, 13 different sources were used for the SHVDB11 and were checked periodically (table 3.1). Other sources were also found, but the kind of information was not precise enough to use them for an accurate validation and are therefore not listed in the table 3.1.

Table 3.1: Ground-truth hail report sources which were used for this project.

Name of the source	Address of the source (contact person)
Insurances	
Schweizerische Hagelversicherung	www.hagel.ch
Vereinigung Kantonalen Gebäudeversicherungen	www.vkf.ch (Herr Markus Imhof)
Luzerner Geäudeversicherung	www.gvl
Online data bases	
Sturmarchiv	www.sturmarchiv.ch
European Severe Weather Database	www.essl.org
SF Meteo Wettermelder	http://www.wettermelder.sf.tv/
Blogs	
Schweizer Sturmforum	www.sturmforum.ch
Meteoradar Wetterblog Schmid	http://www.meteoradar.ch/forum/viewtopic.php?f=10&t=7373
Leimentaler Wetterstation	www.leimentalerwetter.ch
MeteoForum	www.meteoForum.com
Other online sources	
20 Minuten	www.20min.ch
Blick	www.blick.ch
Flickr	www.flickr.com
MeteoSchweiz	www.meteoschweiz.ch
Leimentaler Wetterstation	www.leimentalerwetter.ch
Hike.org	www.hike.org
Bodensee-Feuerwehrebund	www.bodensee-feuerwehrebund.com
Wetterzentrale	www.wetterzentrale.de
Deutscher Wetterdienst	www.dwd.de
Hagelinformation	www.hagelinformation.de
Facebook pdr24	http://www.facebook.com

Every source was graded about its quality and degree of confidence (table 3.2). Grade 4 or higher meant that the observed hail event was sufficient for the project's database and had information about date and location. Grade 5 also included information of time and diameter. 6 was the maximum grade available. These ground-truth observations included images with a scale.

Table 3.2: Criterias which were used to grade the quality of the sources.

Grade	Requirements
1	~date + at least a clue
1.5	
2	~date + ~place
2.5	
3	date + ~place + (time)
3.5	
4	date + place + ~time + (diameter)
4.5	
5	sate + ~ time + place + diameter
5.5	
6	time + place + date + diameter + picture + scale

3.1.2. Information about location

An observation of a hailstorm needs information about the location at least. Otherwise it is not useful. Information about locations of a hailstorm, which were found in Internet, is often insufficient in respect of its accuracy. "Hail between Canton Aargau and Zurich" is not useful, while the report "Hail at Lucerne" is much more precise and was used for the hail database 2011 for instance. Only if the hail observation was related to the commune and its name, the observation itself were used. Hailstorm observations, which included the name of the corresponding commune, were graded with 4 at least (table 3.2). Unfortunately, many of the reports which were found on Internet were about the same event at the same location. No additional information was gained from those multiple observations. Therefore, these locations were only used once. The uncertainty of the reports, whether there was a hail event or not, decreased due to these multiple sources. It is highly unlikely that all these sources about the same location were wrong. It is possible to conclude that events with two or more sources actually occurred. Until the end of the project, 196 different observations had been found for the SHVDB11 with sufficient information about the location.

3.1.3. Information about hail diameter

Fortunately, people also collect information about the hail size. This information is absolutely necessary for a verification of the goodness of MESHS. A lot of them were graded as 5 (in terms of quality) or even higher if there was a picture available on which hail was recognized (table 3.2). Some very motivated storm spotters took pictures with a scale or an object related to a scale. Therefore, they were graded as 5.5 at least or even higher. The minimum grade for them was 4.5 where a sufficient specification of the size could be derived (table 3.2). Altogether, 122 observed hail events with a sufficient indication of size were found.

3.1.4. Data 2009/2010

The Swiss hail insurance⁹ is the national insurer for agricultural losses caused by hailstorms, and has area-wide information of hail events for the last decades. Ground-truth data for the SHVDB09 and SHVDB10 were only used from the Swiss hail insurance and the Lucerne building insurance¹⁰. This means that hailstorm reports for rural and urban areas were available and reduced the risk of missing hail reports on less densely populated areas and missing hail reports due to insufficient sensitivity of certain plants during their seasonal life cycle. In order to determine the false alarm rate these insurance data were very helpful (chapter 3.5).

In total 2538 ground-truth reports of the Swiss hail insurance for the SHVDB09 and 954 for the SHVDB10 were delivered. 7496 ground-truth reports were delivered of Lucerne's building insurance for the SHVDB09 and 800 ground-truth reports for the SHVDB10.

The homogenization of both of these two data sets was a challenge, georeferencing even more. The method of homogenization of these two data sets and the method of georeferencing are described in the next chapters. The Swiss hail insurance and other insurer have information about hail losses and their corresponding locations in their archives. Unfortunately, insurers do not collect data about hail size. Therefore, it was necessary to collect data for the SHVDB11 during the hail season to get information about the hail sizes, otherwise, the validation of MESHS could not have been accomplished.

Kessinger et al. (1995) used 237 different ground-truth reports. 107 reports were used by Witt et al. (1998), 40 reports were used by Schiesser et al. (1999) and approximately 2100 ground-truth reports were used by Holleman et al. (2001). Wilson et al. (2009) used a data set of 3921 observation reports.

3.1.5. Data 2011

Data which were collected for the SHVDB11 (May–September) were systematically recorded in an evaluation table (verification_data_2011.xls). In total 196 different ground-truth reports of different sources (3.1.1) were collected. Events before or after the season are very rare. The evaluation table includes compulsory information on observed hail events such as date, location, name of the canton where the hail events 2011 occurred, name of the source and the grade of the source. Additional information, such as the time of the hail event, duration, observed average diameter of the hail stones, were included if these kinds of information were available. Note that only reported hail events could be collected for the SHVDB11. For less densely populated areas it is likely that hail events were missed. Hail observations which were not reported are not a proof that no hail occurred at those areas. Therefore, it is possible to conclude where hail was falling but it is not possible to conclude where no hail was falling (e.g. Holleman, 2001; Hyvärinen et al., 2010). The final evaluation table contains Swiss

⁹ <http://www.hagel.ch>

coordinates and world coordinates (UTM/WGS84) for each single hail observation, to use them for visualization in Google Earth. Further explanations about the methods of georeferencing can be found in chapter 3.3. Explanations of the categories of the evaluation table were inserted in the appendix (table 7.1).

3.2. Radar data

For this study, radar data were only used in GIF format. POH and MESHS algorithms also use the height of the 0°C layer of MeteoSwiss's COSMO-2 model (hzero). Hzero files are calculated with hourly temporal resolution.

Beside the real-time output products with 5 minutes resolution, 24 hours outputs, as integration of the maximum occurred values of a certain day, are computed as well. This daily hail outputs integrate the maximum detected hail signal for each day and each pixel from 00.00–23.55 UTC. Accordingly, the maximum detected value of each pixel is shown.

The collected ground-truth hail data allow assessing the hail detection algorithms on a daily basis. The SHVDB09/10 include information about the day and corresponding commune of a certain hailstorm. The SHVDB11 gives more detailed temporal information, but not all of them. Therefore, a commune-based verification on a daily basis was possible. A higher temporal resolution was not applied. The general temporal tolerance of the data sets was 00.00–23.55 UTC for each day. Hail events which occurred beyond this time window were compared with the daily integrated output of the next day.

Finally, the daily integrated plots simply show the situation of a certain day. The SHVDB09/10 are not given information whether a commune was hit once or more by a hailstorm. The time when the hail observation is reported is not crucial. If an observer notifies the occurrence of hail with the right date, this observation will be automatically verified with the right daily output. The analysis showed that the radar-based hail detection outputs corresponded well with the ground-truth data sets. It was not necessary to attend the ground-truth data of previous or the next days. This in turn means, that the temporal tolerance was defined as 00.00–23.55 UTC for each day. Hail events before this time window were compared with the daily integrated plots of the previous day. Hail events after this time window were compared with the daily integrated plots of the next day.

It could be that hail observations belong to another hail event than observed by radar. But investigations have shown that ground-truth data mostly belonged exactly to one single hail swath. Therefore the problem was not considered further.

¹⁰ <http://www.gvl.ch>

3.2.1. Radar-based hail data 2011

For the hail season 2011 (May-September) the different hail products were available as daily integrated GIF outputs and data files (.dat). The daily POH, MESHS and HAIL outputs were used as described in the next chapters.

3.2.2. Radar-based hail data 2009/2010

Calculating daily integrated outputs of POH and MESHS have been started operationally in 2011. Daily integrated hail outputs for 2009 and 2010 were not available, except for the HAIL algorithm. In order to improve the size of the archive, recalculations had been done. Among other things, that also was one of the objectives of this study.

3.2.2.1. Recalculation of POH and MESHS outputs for 2009/2010

This section describes briefly the recalculation of the POH and MESHS outputs of 2009 and 2010. More detailed information is given in the manual of the recalculation program (manual POH_MESHS_recalculation).

Only the COSMO-2 hzero files of the time interval when hail occurred have been saved in the archive. To calculate daily hail outputs from 00.00–23.55 UTC all 24 hourly hzero files are necessary. In order to recalculate these daily integrated hail files, it was assumed that the 0°C height did not change dramatically during a day and therefore the hzero height is constant. The earliest and latest hzero files of each hail day were used to create the other missing files.

As mentioned in chapter 3.3, Google Earth was used in order to illustrate radar images and ground-truth observations in a simple, intuitive and user friendly way. The extended version of the recalculation program (POH_MESHS_recalculation_ge.sh) also includes a part to create KML (.kml) files for Google Earth automatically.

3.3. Visualization

Radar images and ground-truth hail observations were visualized using Google Earth (figure 3.1). Google Earth is an open source application that streams high-resolution static satellite imagery and map overlays to a 3D display on a user's desktop. User generated products may be shared over the Internet. Because Google Earth is an application that runs on inexpensive hardware, it provides an easy way to view weather products that are disseminated over the Internet (Smith et al., 2006).

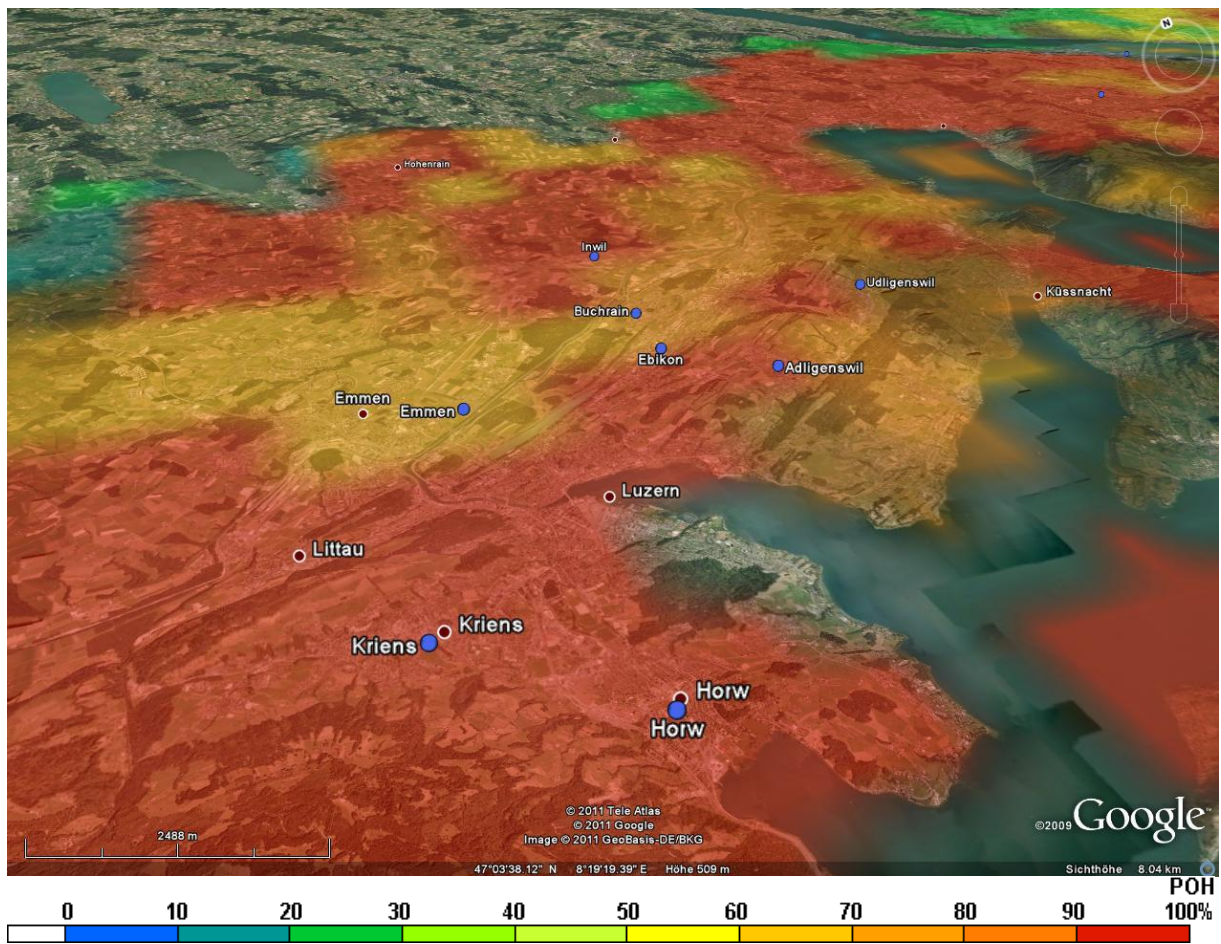


Figure 3.1: Ground-truth hail reports (blue points) and daily integrated POH output visualized in Google Earth. In this example the region of Lucerne is shown with POH and hail observations of July 22 2011.

Google Earth has been used in several studies for verification of hail detection algorithms (e.g. Ortega et al., 2006, 2009; Wilson et al., 2009). It can quickly be recognized where a hail event occurred. The zoom function allows identifying which communes were affected of the hail swath and which not.

3.3.1. Georeferencing observations

The SHVDB11, SHVDB10 and SHVDB09 were included in Google Earth. SHVDB11 data, which had been collected on Internet, were georeferenced separately. The service of Retorte¹¹ was very helpful in order to determine the coordinates in UTM and Swissgrid. The SHVDB09/10 were georeferenced automatically. The Swiss Federal Office of Topography (Swisstopo) provides all coordinates of each of Switzerland's communes. Therefore this data file was used.

In a first step, all hail observations of the same date and same commune were summarized as one single observation. Ground-truth observation of the Canton Lucerne showing in Google Earth, which mostly coming from the building insurance, includes sometimes hundreds of single observations, but are visualized as one single point.

In a second step, the summarized communes were connected with the Swisstopo coordinates. In order to obtain UTM coordinates for Google Earth, the Swiss coordinates were converted into UTM coordinates. Swisstopo provides different online tools which allow converting different coordinate systems and data formats¹². The transformation process will easily be managed if the tables are used in text (.txt) format or csv (.csv) format. After that, ground-truth observations were inserted in Google Earth. Unfortunately the automatic allocation sometimes failed. Ground-truth observations were allocated with wrong coordinates. These had to be removed manually. In total 3644 different ground-truth hail observations were visualized automatically as points in Google Earth, 2553 for 2009, 898 for 2010 and 196 for 2011. After removing the wrong georeferenced points approximately 3500 ground-truth data are visualized in Google Earth. In order to compute the corresponding data set for Google Earth, the online tool of Earthpoint¹³ was used. There, tables can be transformed in KML files. These were prepared for the transformation. One header line had to be inserted (table 3.3). Earthpoint read the header and computed the KML file. Unfortunately, maximum 200 single points can be submitted to the Earthpoint server. For these days, which included more than 200 different ground-truth observations, the table had to be separated and then sent to Earthpoint. The corresponding KML files were merged again in Google Earth.

¹¹ <http://tools.retorte.ch/map/>

¹² <http://www.swisstopo.admin.ch/internet/swisstopo/de/home/apps/calc/reframe.html>

¹³ <http://www.earthpoint.us/ExcelToKml.aspx>

Table 3.3: Example of the header (1st line) of the excel table of July 07 2011. Latitude and longitude are coordinates in the UTM system. Name is the name of the communes. Icon is the key word for Earthpoint to compute all ground-truth observations with the chosen symbol. IconColor are the colors which were chosen in order to distinguish the different hail events. IconScale is the key word to change the diameter [cm] of the ground-truth symbol in Google Earth. HTML color names can be used¹⁴

	Latitude	Longitude	Name	Icon	IconColor	IconScale
07.07.2011	47.05022	8.31012	Luzern (LU)	301	Darkorange	1
07.07.2011	47.06326	8.27987	Reussbühl (LU)	301	Darkorange	1
07.07.2011	47.12812	8.74427	Einsiedeln (SZ)	302	Darkorange	1.25
07.07.2011	47.26006	8.85324	Rüti (ZH)	302	Darkorange	1.25
07.07.2011	47.17039	8.7626	Etzel (SZ)	302	Darkorange	1.25
07.07.2011	47.01983	8.6474	Schwyz (SZ)	302	Darkorange	1.5
07.07.2011	47.69662	8.45724	Hallau (SH)	302	Darkorange	1.5
07.07.2011	47.17459	8.51385	Zug (ZG)	302	Darkorange	1.5
07.07.2011	47.39077	8.17345	Lenzburg (AG)	303	Darkorange	1.65

In order to distinguish the observations of different years and hail events, individual colors were defined for the events. Each data point was named with its corresponding commune and Canton (in brackets). The visualized ground-truth data cannot be distinguished any longer from which source they are coming from. Only different hail events can be distinguished.

122 data points of the SHVDB11 also include information about hail size. Those data points were represented in different diameters and were declared with the category of this certain hail diameter. Smallest diameters were used for ground-truth data without information about size. The higher the diameter of the data point in Google Earth, the higher was the diameter of the collected hail stone. Figure 3.2 a) shows an example of ground-truth hail observations in Google Earth.

Further, visualized ground-truth observations were also numbered with its corresponding size of the category. Figure 3.2 b) shows the categories used in Google Earth. Accordingly, each number indicates the maximum possible hail size [cm] within this category.

¹⁴ http://www.w3schools.com/html/html_colornames.asp

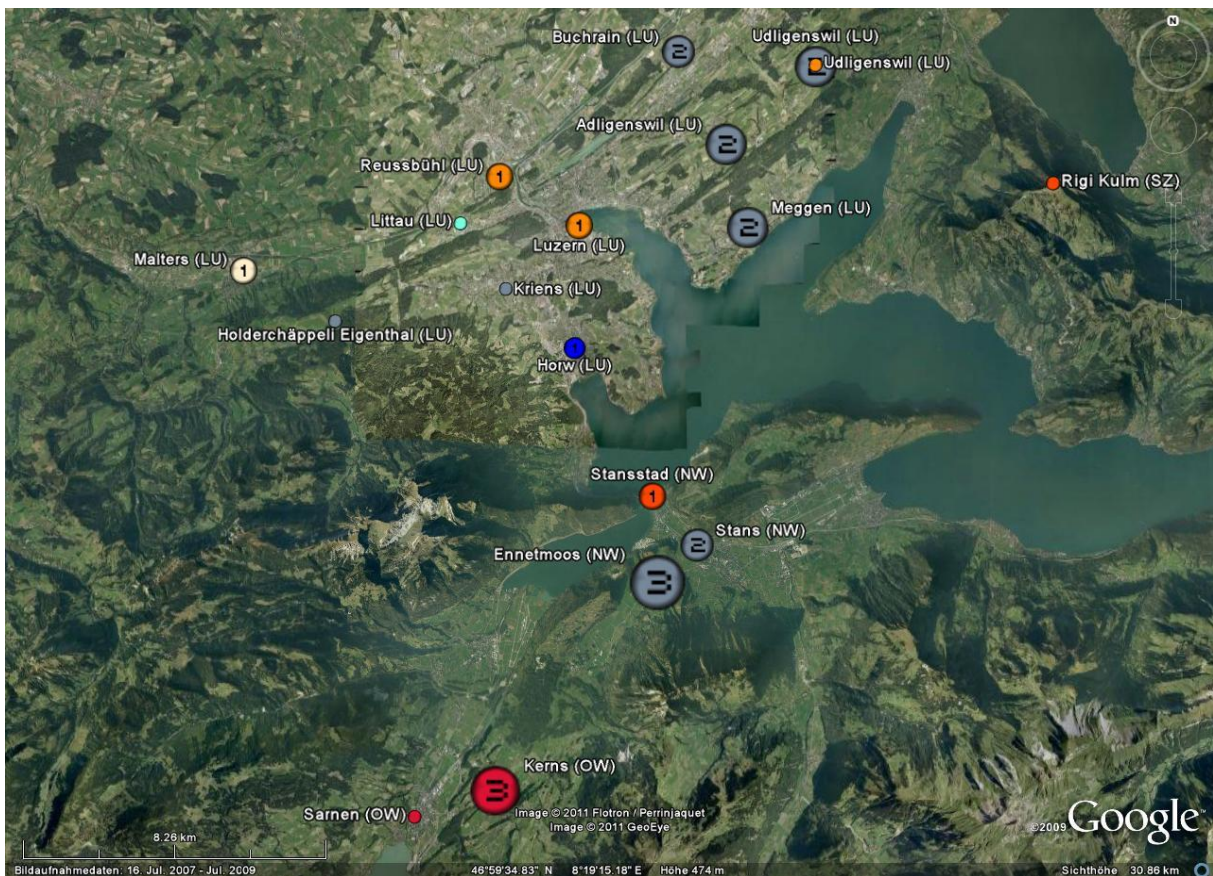


Figure 3.2 a): View on the Lake Lucerne with visualized ground-truth hail observations of 2011. Each color represents an individual hail event (hail swath). Points without numbers are observations without any information about hail size. Diameters of the data points increase with increasing observed hail diameter. The scale is shown in figure 3.2. It can be recognized clearly that the data point Ennetmoos (NW) is slightly larger in diameter, due to the larger observed hail size, than Kerns (OW), but were allocated in the same size category.

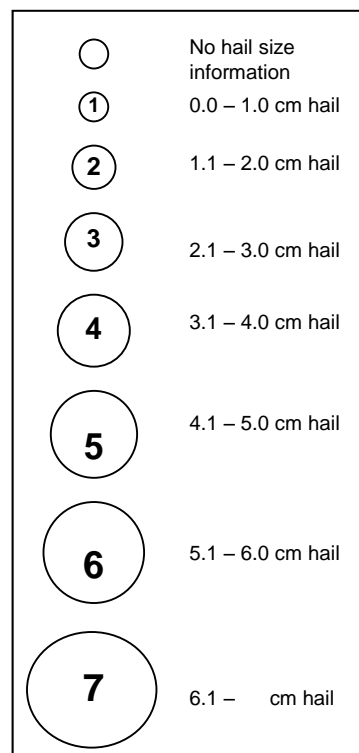


Figure 3.2 b): Size scale of the data points which was used in Google Earth.

3.3.2. Georeferencing of radar images

Images can be imported in Google Earth as overlays. Different formats are supported. For this study the radar images were used as GIF files. The images were overlaid over the area of Switzerland. A ground-based overlay was used. Images can also be imported as hovering images over the ground. The ground-based overlay was chosen in order to use the zoom function of Google Earth. Otherwise, the image layer over the ground is not visible when zooming closer to the ground.

In Google Earth two different georeferencing methods can be applied. The first one georeference the image overlays with the coordinates of each of the four edges of an image. The second method uses pass points. With this method distinctive points are used to fix the image on the ground. The pass point method was used for this project. Therefore, the border of Switzerland was used as pass points. The overlay image itself must have a North-Top orientation with simple cylindrical projection. Other projections also are adequate enough while overlay only a small area. For Switzerland this restrictions does not affect. Switzerland is a small country. Distortions due to a non-cylindrical projection are small. The radar images were overlaid in such a way that the distortions are smallest in northern part of Switzerland and highest in the southern part and Canton Grisons. There are nearly no distortions in the north-south axis but in the east-west axis. For the region of Chiasso maximum distortions of 2 km appeared (figure 3.3). Note that Google Earth was only used for visualization. The distortion did not affect the verification process but is explained here in terms of completeness.

First georeferenced KML (.kml) files were created. For these templates original daily integrated output files of POH, MESHS and HAIL were overlaid in Google Earth. These overlays were saved as KML files. The KML files included the coordinates which were used for further implementations.

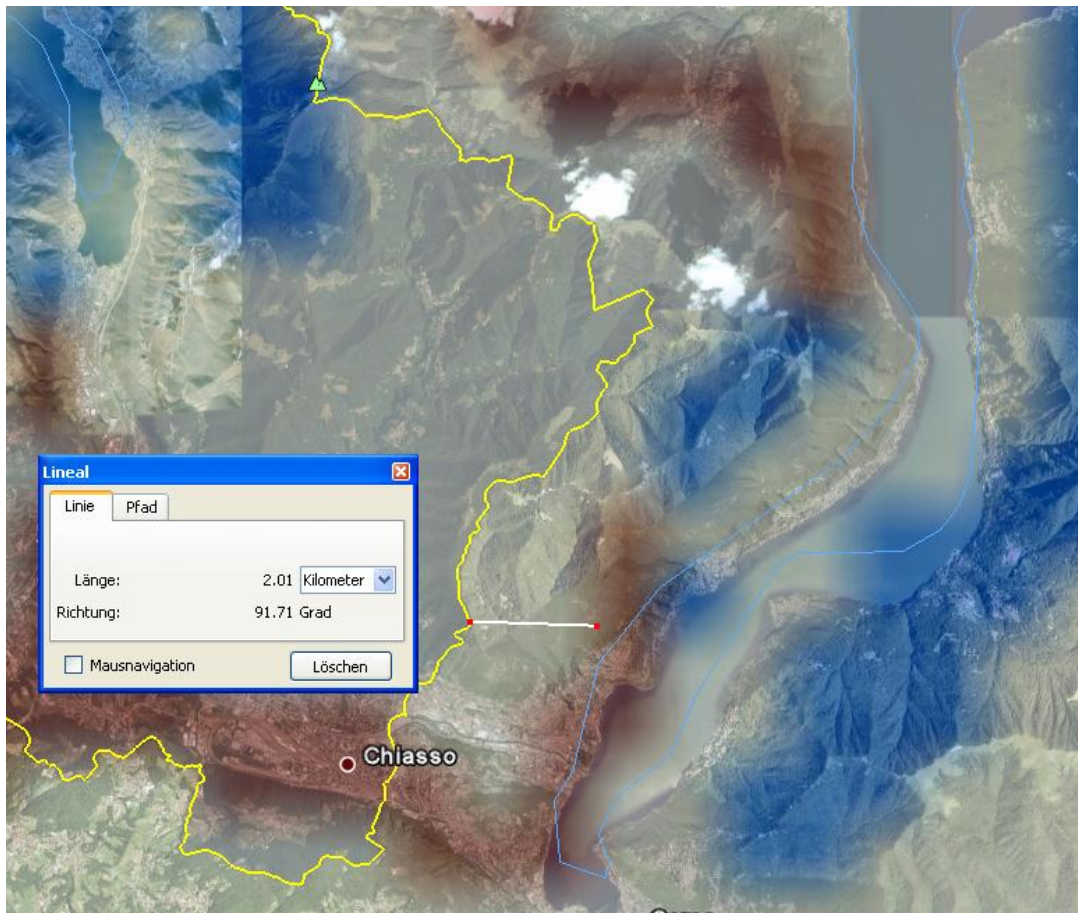


Figure 3.3: Map of the region of Chiasso in southern Switzerland. The white line shows the distance of maximum distortion in east-west direction. The length of the line is 2.01 km.

3.3.3. Adaption of radar images for Google Earth

The daily integrated outputs of POH, MESHS and HAIL had to be adapted for further use in Google Earth. These output files of POH, MESHS and HAIL were adapted in IDL in order to make all these pixels transparent, which are not part of the radar signal. After this step the corresponding KML file of each of these transparent POH, MESHS and HAIL files was created. A schematic illustration is shown in figure 3.4.

In order to import these radar outputs in Google Earth two different programs were written. The program `make_kml.sh` computes KML files of all recalculated files, which were calculated with the program `POH_MESHS_recalculation_original.sh`. The program `hailge_operational.sh` allows computing a KML file for each of the three hail products from the MeteoSwiss daily quickload archive. Further explanations can be found in the manuals of the programs (manual `POH_MESHS_recalculation`; manual `hailge`).

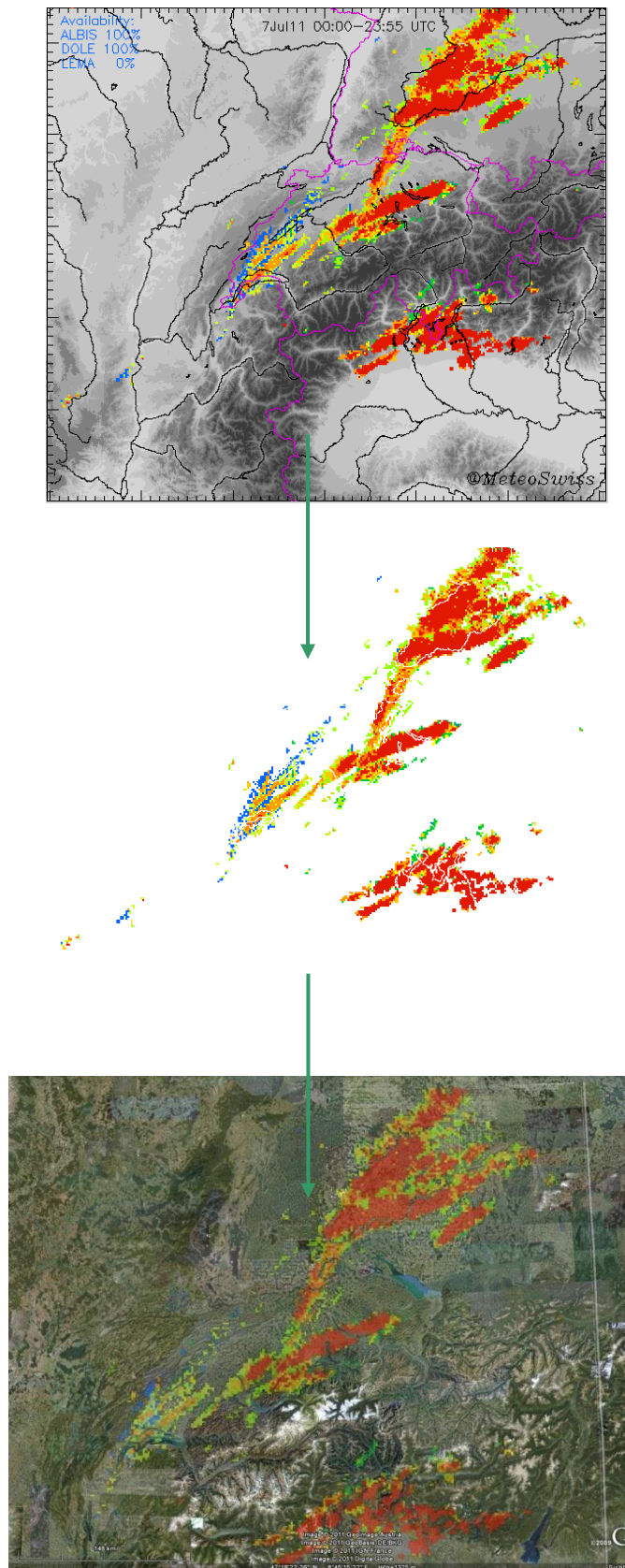


Figure 3.4: Schematic illustration of the computation from a daily integrated GIF output file of a POH output to a Google Earth overlay for the July 07 2011. The green arrows show the direction of computing. The picture on the top was transformed to KML file using IDL.

3.3.4. KML-file for Google Earth

The radar image overlays in Google Earth were adapted in respect of their transparency. A transparency of 60 % was used for this project (keyword color in KML code). Accordingly, radar overlays and the Google Earth map are visible at the same time. That was very helpful to determine which commune was affected by a hailstorm or not. The structure of the KML files is simple. Important information can be found on the Google Earth supporting page¹⁵. In the following, an example of the POH radar overlay of July 07 2011 is given.

```
<?xml version="1.0" encoding="UTF-8"?>
<kml
xmlns="http://www.opengis.net/kml/2.2"xmlns:gx="http://www.google.com/kml/e
xt/2.2"
xmlns:kml="http://www.opengis.net/kml/2.2"xmlns:atom="http://www.w3.org/200
5/Atom">
<GroundOverlay>
  <name>POH_07.07.2011</name>
  <color>7dffffff</color>
  <Icon>
    <href>//lomnas200.meteoswiss.ch/home/lom/users/plom01/My
    Documents/Hailvalidation/Validation/Google
    Earth/radar_overlays/POH_11/POH11188_trsp.gif</href>
    <viewBoundScale>0.75</viewBoundScale>
  </Icon>
  <LatLonBox>
    <north>49.08098891603251</north>
    <south>44.23598720776022</south>
    <east>11.48696597374529</east>
    <west>3.464063047376122</west>
    <rotation>-0.1716467492878798</rotation>
  </LatLonBox>
</GroundOverlay>
</kml>
```

Additional information can be found in the corresponding manual of the programs (manual hailge; manual POH_MESHES_recalculation).

3.3.5. Kmz-file for Google Earth

Beside the KML format Google Earth also support the KMZ (.kmz) format. The KMZ format is a highly compressed format. It is very useful in order to share the Google Earth files with other users. KMZ files cannot be edited directly. Google Earth has to be used for editing. All hail events of 2009, 2010 and 2011 with its corresponding ground-truth reports and radar outputs were summarized in the Google Earth file 'Hail Switzerland 2009, 2010, 2011.kmz'.

¹⁵ <http://www.google.com/earth/index.html>

3.3.6. Animation POH and MESHS in Google Earth

Radar images of any radar product usually are animated in order to recognize the direction and velocity of the specific fields. Animations can also be done in Google Earth. For this project two cases were animated. The first case was a hail event on August 24, 2011. The second case was a hail event on September 11, 2011. For both cases POH and MESHS were animated (anim_POH.pl, anim_MESHS.pl, anim_POH4.pl). Further information can be found in the corresponding manuals. The animations can be found in the KMZ file (hail Switzerland 2009, 2010, 2011.kmz/hail 2011/radar_overlays_2011/animations_11).

3.4.3x3 verification matrix

In order to calculate statistical numbers such as probability of hail (POD) or goodness of MESHS, radar images and ground-truth hail observations were compared in a systematic way. For this analysis, a 3x3 verification matrix was used. The GIF outputs of the radar were overlaid with this 3x3 verification matrix for each observed hail event (figure 3.5). As mentioned in chapter 3.3 each hail observation was georeferenced with world coordinates (UTM/WGS84) and with Swiss coordinates (Swissgrid). These coordinates were used to place the matrix in such a way that the central pixel of each 3x3 matrix included the coordinates at which location the corresponding hailstones were observed and also was compatible with the radar grid. These central pixels were defined as mid-pixels. The other pixels were named vicinity pixels. Figure 3.6 shows that for each hail location an area of 36 km² was covered by the verification matrix. The spatial tolerance within a pixel was maximum the square root of the pixel size and therefore ≈ 3 km (figure 3.5). While it is assumed that the ground truth report is georeferenced very accurately (error ~ 0 m), it is the radar pixel that has to define the spatial uncertainty. Setting the spatial tolerance to ~ 1.5 times the actual radar pixel dimension is a conservative estimate of measurement uncertainty. Therefore, the final verification results also represent a rather conservative estimate of the performance of the algorithms.

$$\text{Spatial tolerance} = 2 * \sqrt{2} = 2.83 \approx 3 \text{ km}$$

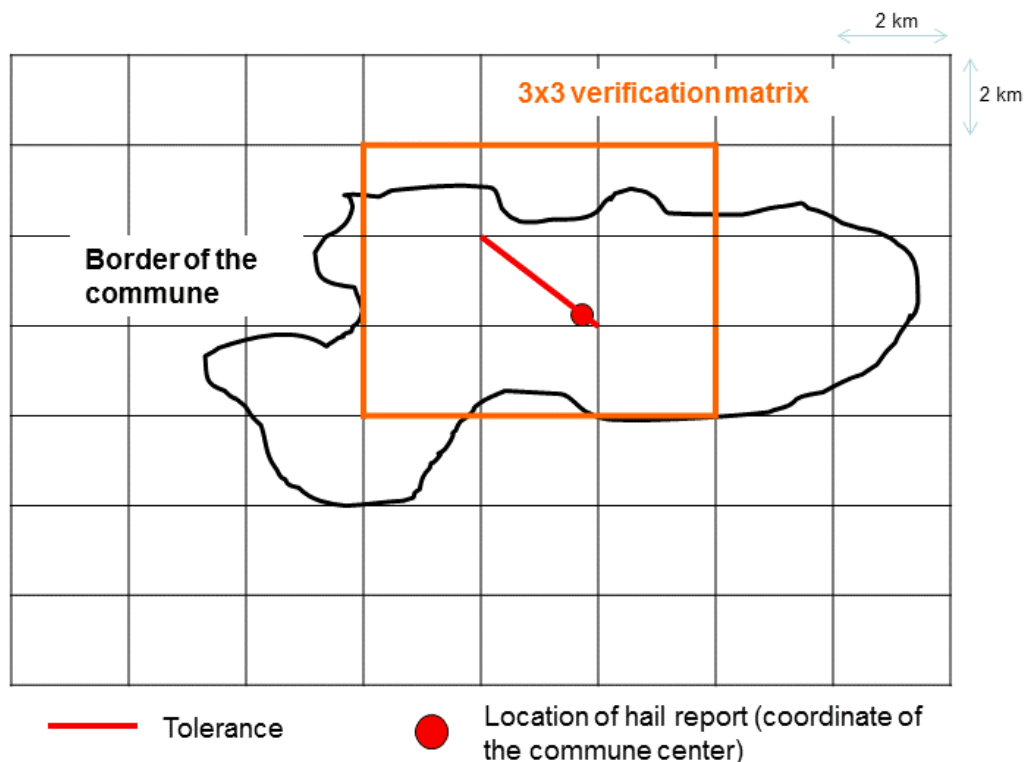


Figure 3.5: Schematic of the placement of verification matrix (orange) and the maximum tolerance from an observation (red point) to the most far radar pixel (red line).

This is in line with other studies, which used spatial tolerances up to 30 km (Kessinger et al., 1995; Witt et al., 1998; Holleman et al., 2001; Wilson et al., 2009; Hyvärinen et al., 2010).

The GIF outputs of the hail algorithms were adapted in order to apply them for the verification. A filter was used to select pixels which contain information about hail. According to chapter 3.5.1, pixels of the outputs which do not show information about hail (grey-shaded) were set equal 0. Therefore pixels with values > 0 (colored) were counted as hit and values < 0 were classified as miss pixels. In order to count a ground-truth hail observation as detected due to the radar, at least one pixel of the whole verification matrix had to be included a radar-based value > 0 . Otherwise, if the whole matrix only included radar values equal 0 (grey-shaded values), this matrix was classified as miss, which means that the given radar algorithm was not able to detect the corresponding hail event at a given location in a sufficient way. Therefore, one radar pixel within the matrix is enough to count the ground-truth observation as detected due to the specific algorithm (Figure 3.6). The verification itself is based on the “eyeball” principle. Every single location was undergo a visual control.

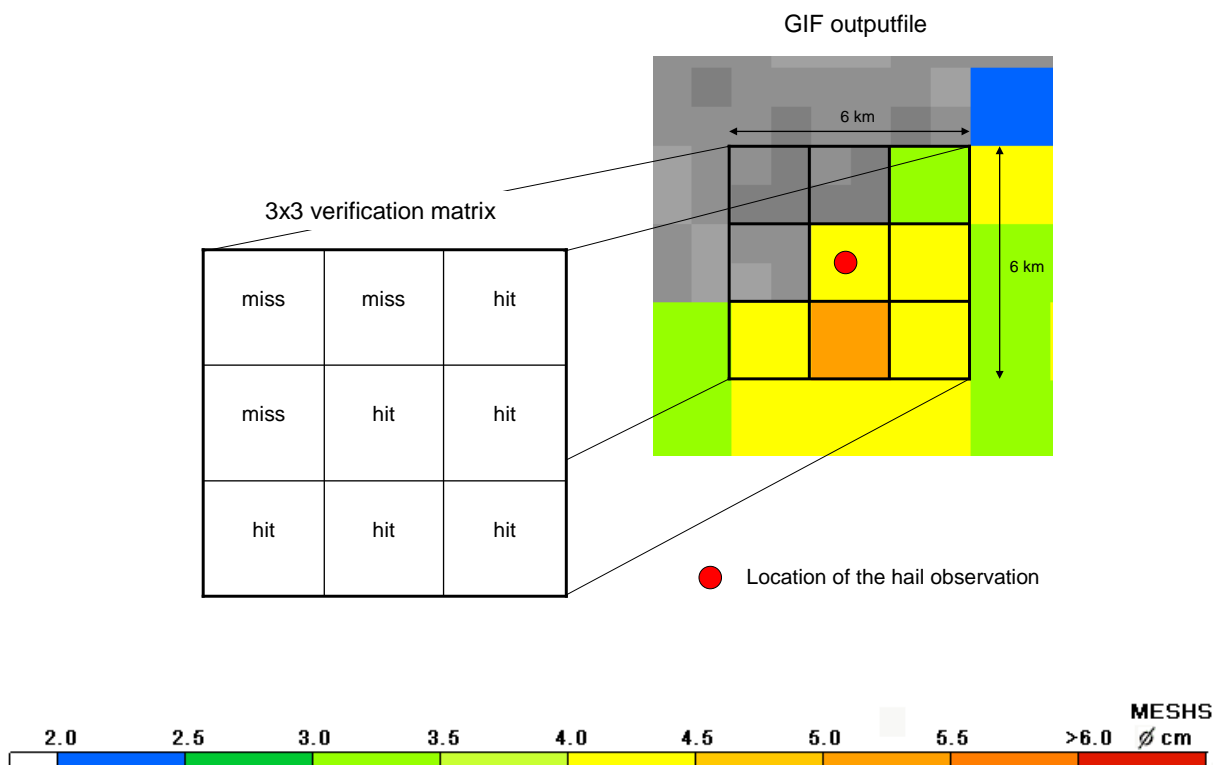


Figure 3.6: Schematic of the verification process with a 3x3 verification matrix. The output files as GIF were calculated from POH, MESHS or HAIL. Each grey colored pixel was counted as miss in the matrix. Blue, green, orange and yellow colored pixels were counted as hit.

The values of each verification matrix which were calculated for the different hail event sites of the year 2011 were collected in a table. In addition to the information hit or miss of the pixels, the quantitative numbers of each pixel were also collected in this table. The POH algorithm gives information in %, the MESHS algorithm in cm and the HAIL algorithm gives simply a categorization whether hail is probable or possible (figure 3.7).

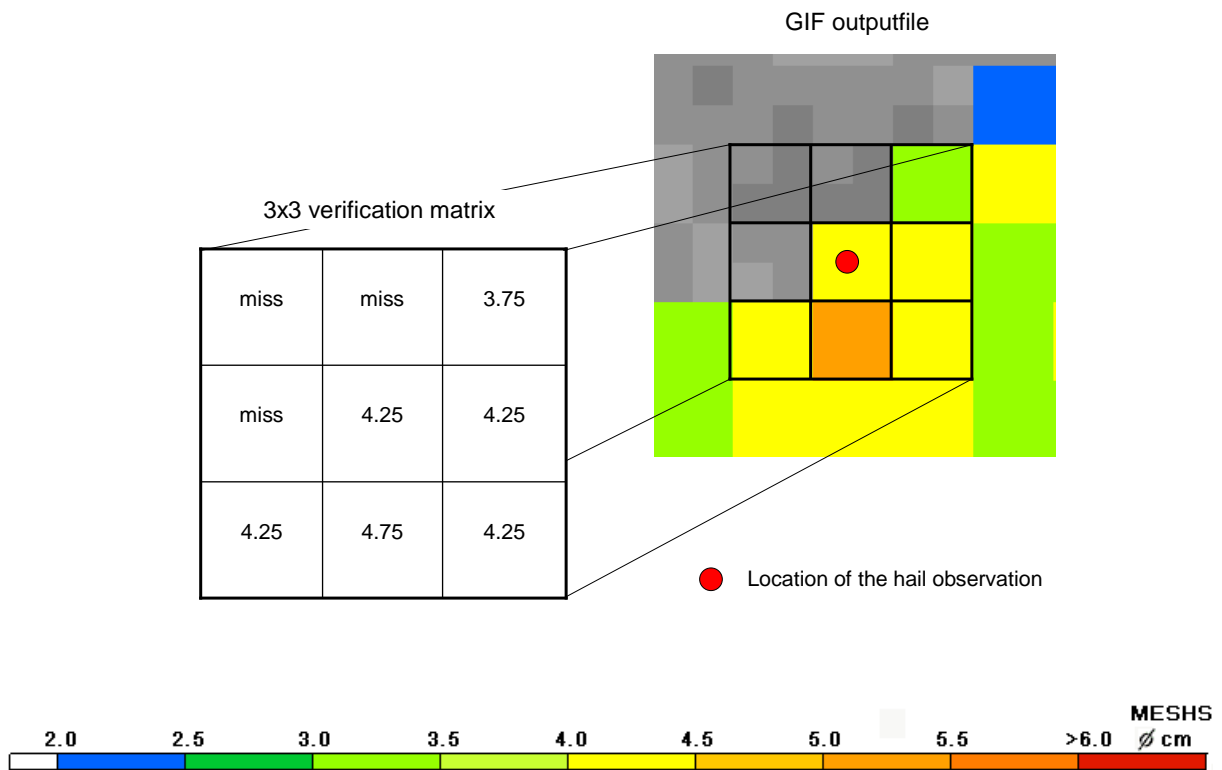


Figure 3.7: Schematic of the verification process with a 3x3 verification matrix. The output files as GIF were calculated from POH, MESHES or HAIL. Each colored pixel was counted with its quantitative value (in this case value of MESHES [cm]).

With the help of this table the average, median or minimum and maximum values were calculated. In order to define the correlation between the radar-based MESHES values and the ground-truth hail data, values such as deviation had to be computed as well. For each radar-based hail algorithm, maximum and minimum output values were defined simply as the highest or lowest value within each 3x3 verification matrix. Average and median were calculated from the quantities within these verification matrices. Pixels with values equal 0 were not used for statistics. Sometimes, the GIF outputs were overlaid with the border of Switzerland, lake contours or rivers. Therefore, it was not possible to distinguish between hit, miss or quantitative values. In order not to lose the information about the number of pixels which were used for each matrix, these quantities were collected as well.

The deviation of POH was calculated as the difference between 100 % probability of hail and the median of POH due to the calculations of the 3x3 verification matrix (equation 3.1).

$$\textit{Deviation of POH} = 1 - \textit{POH}_{\textit{median}} \quad (3.1)$$

It was difficult to quantify the deviation of the HAIL algorithm. Therefore, the category HAIL possible was graded with 1 and HAIL probable with 2. Average and median give an estimate whether HAIL detected the hail event closer to the category HAIL probable or HAIL possible.

Deviation of MESHS was calculated as shown in equation 3.2.

$$\text{Deviation of MESHS} = \text{MESHS}_{\text{median}} - \text{Max. Diameter} \quad (3.2)$$

The number of pixels with values > 0 within verification matrices can be an indicator whether a certain hail event occurred on the border of a hail cell or in the core. If a matrix just include one radar pixel with information about hail, it is probable that an event happened at the border of the hail cell.

More information about the different classes which were calculated are given in table 7.1 in the appendix.

3.5. Verification scores

3.5.1. Contingency table

Scoring parameters are important quantities and allow comparing different hail events and hail seasons with each other. Scoring parameters can be defined with a contingency table (figure 3.8). Hail detected by a radar-based method which is confirmed by the verification data will be classified as a hit (*H*), hail detected by a radar-based method which is not confirmed by verification data as a false alarm (*F*), hail observations or reports in the verification data that are not detected by the radar-based method as a miss (*M*), and no event at all a non-event (*N*) (Holleman, 2001; Donaldson et al., 1975).

	Hail	No hail
Radar detection	H	F
No radar detection	M	N

Figure 3.8: 2-by-2 contingency table for hail verification process.

3.5.2. Probability of Detection

The probability of detection (POD) is the most important scoring parameter in order to do verifications. The probability of detection and the false alarm rate (FAR; in chapter 3.5.3) always have to be used together to characterize the results of a verification, where the method with a high POD and a low FAR is preferred (Holleman, 2001). For this study PODs were calculated for the years 2009, 2010 and 2011. In total 54 different hail events were analyzed, 32 hail events of 2011, 10 hail events of 2010

and 12 hail events of 2009. The probability of detection is defined, using a 2x2 contingency table (figure 3.8), as follows (equation 3.3):

$$\text{POD} = \frac{H}{H + M} \quad (3.3)$$

The overall POD is weighted with the number of ground-truth reports in order to give all reports the same priority. The average is not use due to the fact that small events (with less ground-truth reports) are not of the same importance than severe hail events (with lots of ground-truth reports).

3.5.3. False Alarm Rate

The false alarm rate (FAR) is an important scoring parameter and should always be used together with the POD. The false alarm rate is defined, using a 2x2 contingency table (figure 3.8), as follows (equation 3.4):

$$\text{FAR} = \frac{F}{H + F} \quad (3.4)$$

For this study a more observation-based perspective was applied in order to compute the FAR. Therefore, the SHVDB09 and SHVDB10 were used. SHVDB11 was sufficient in order to determine the probability of detection (POD) with an observation-based perspective. But 196 observations are not sufficient enough to determine whether a radar pixel is a false alarm pixel or not. The SHVDB09 and SHVDB10 include much more data points, therefore FAR was taken into account for these two years only. Otherwise, huge areas would be counted as false alarm areas (FAA) due to missing ground-truth hail observations. This risk is reduced for data-set with more data-points.

The FAR was determined from an applied point of view. For a prediction of hail swaths within the next hours, not the single pixels were considered. It is much more important to predict the path of the main hails swaths. According to this, a hail swath perspective was used (hail swath ≥ 10 continuous pixels) and therefore a hail-swath-based FAR was computed. The hail swath perspective was also used by Ortega et al. (2006, 2009).

For each of the two data bases (SHVDB09, SHVDB10) the main hail swaths were determined in Google Earth. An additional layer with the population density of Switzerland (2000) was imported in Google Earth (figure 3.9).

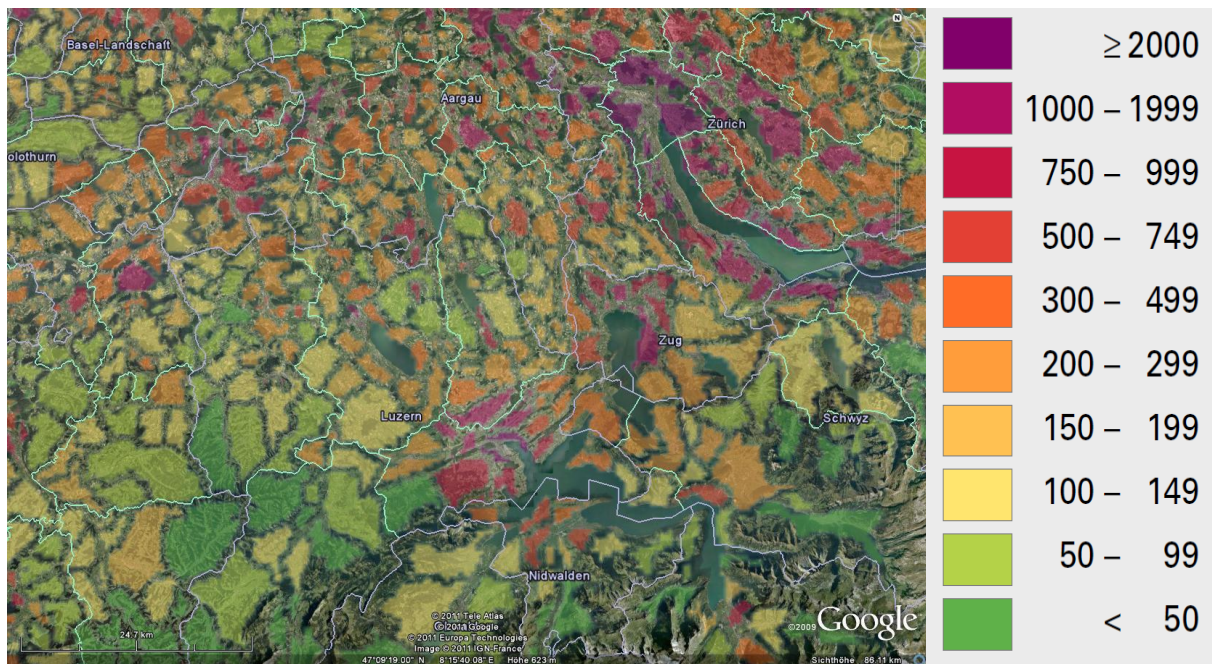


Figure 3.9: Population density map in Google Earth per km² of the productive area of Switzerland. The corresponding legend can be seen on the right side. In this image the region of Lucerne, Zug and Zurich are shown.

Hail swath areas (≥ 10 continuous pixels) with population density between 100 and 749 persons per square meter were determined and corresponding polygons for further calculations were drawn. Communes with population density <100 and >749 persons per square meter were not considered due to the fact, that these areas are low populated or urban areas and are not sensitive to the assessment of the Swiss hail insurance (except agglomeration of Lucerne where data of the Lucerne's building insurance were available). After that, the ground-truth observations were plotted over these polygon areas. Sections without any ground-truth points were defined as false alarm areas (FAA). A more detailed insight of the rules which were used for this verification is shown in figure 3.11.

The program Google Earth Pro was used to calculate the areas of the hail swath polygons and the FAA. For every single hail event which included hail swaths the false alarm rate was computed. Therefore, the following formula was used (3.5).

$$\text{FAR}_{\text{hail swath}} = \frac{F_{\text{hail swath area}}}{F_{\text{hail swath area}} + H_{\text{hail swath area}}} \quad (3.5)$$

The overall FAR (weighted with the considered area) was calculated as the sum of all false alarm areas [km²] divided by the sum of all hail swath areas [km²] (formula 3.6). Figure 3.10 shows the hail swath polygons of June 06, 2009 (green) and the corresponding false alarm areas (red).

$$\text{Overall FAR}_{\text{hail swath}} = \sum \frac{F_{\text{hail swath area}}}{F_{\text{hail swath area}} + H_{\text{hail swath area}}} \quad (3.6)$$

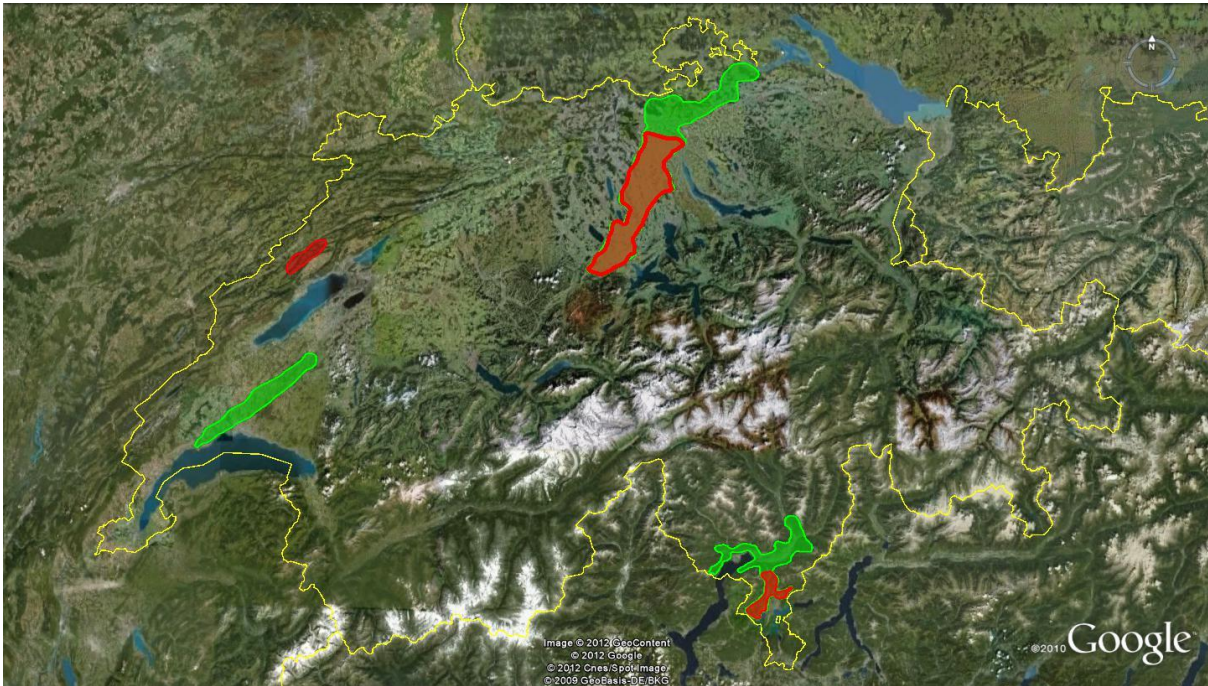


Figure 3.10: Hail swath polygons for FAR determination of June 06 2009. Green polygons are areas where hail occurred over settled areas. Red areas are polygons, where no ground-truth report was found within the green polygons. Red polygons are false alarm areas (FAA). The yellow line is the Swiss border.

Hail verification tree

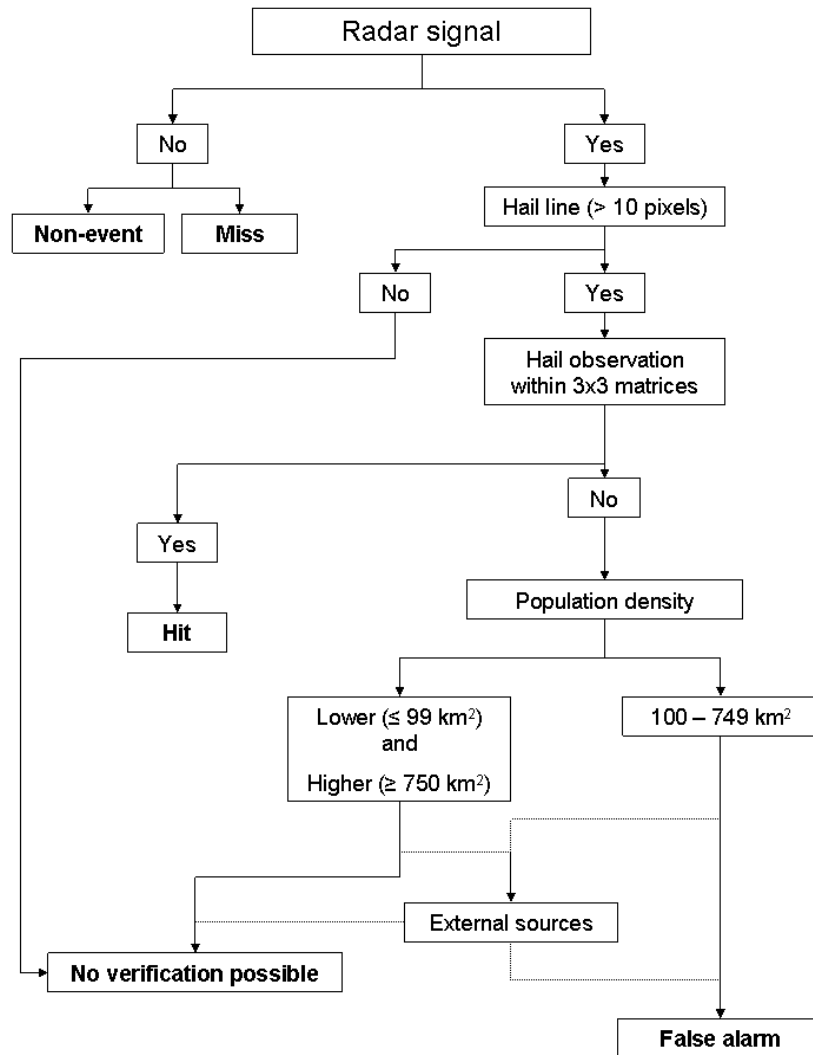


Figure 3.11: Schematic of the verification process, used for the determination of false alarm rates (FARs).

3.5.4. Critical success index

Beside the two scoring parameters POD and FAR the critical success index (CSI) were used. The CSI characterizes the verification results in a single number. The higher the CSI value the better the method. The CSI is defined, using a 2x2 contingency table (figure 3.8), as follows (equation 3.7):

$$CSI = \frac{H}{H + M + F} = \left[\frac{1}{POD} + \frac{1}{1 - FAR} - 1 \right]^{-1} \quad (3.7)$$

Within hail verification studies the CSI is a common criteria and therefore used for this study as well. But the CSI has the disadvantage that it rewards the detection or prediction of an event with a high frequency. Overdetection or overforecasting is then the case. Therefore, the bias should be used to identify this overdetection or overforecasting (Holleman, 2001).

For this study CSI was computed with the SHVDB09/10. In total 22 events with 2408 ground-truth reports were analyzed, 12 hail events with 1746 ground-truth hail reports of 2009 and 10 hail events with 662 ground-truth hail reports of 2010.

3.5.5. Bias

The bias is the ratio between the number of detections or forecasts and the number of actual occurrence. It is a quantity which shows the systematic error within a calculation. A method that detects or predicts events with a too high frequency has a bias greater than one. A bias smaller than one means that a method detects or predicts events with a too low frequency. A method with a bias of one has no bias. In order to compute the bias the data for CSI computing was used. The bias is defined, using a 2x2 contingency table (figure 3.8), as follows (equation 3.8):

$$\text{bias} = \frac{H + F}{H + M} = \frac{POD}{1 - FAR} \quad (3.8)$$

3.5.6. Goodness of MESHS

In order to evaluate the correlation between the MESHS output and ground-truth hail observations of the year 2011, both were plotted against each other and the coefficient of determination (r) (equation 3.9) was calculated.

$$r_{xy} = \frac{\sum_{i=1}^n (x_i - \bar{x})(y_i - \bar{y})}{\sqrt{\sum_{i=1}^n (x_i - \bar{x})^2 * \sum_{i=1}^n (y_i - \bar{y})^2}} \quad (3.9)$$

4. Results

4.1. Verification scores

4.1.1. Verification scores 2009

Table 4.1 shows the calculated POD, FAR, CSI and bias scores for all 11 considered hail events of 2009. An overall POD of POH (weighted with the number of ground-truth reports) of 97% was found with maximum values of 100% and minimum values of 85%. An overall FAR of POH (weighted with the considered area) of 19% was found with maximum values of 41% and minimum values of 8%. The CSI of POH shows values from 89% to 55%. An overall CSI of POH of 79% was calculated. The overall bias of POH was for all events (excepted June 22th) greater than 1. An overall POD of MESHS (weighted with the number of ground-truth reports) of 87% was found with maximum values of 94% and minimum values of 36%. An overall FAR of MESHS (weighted with the considered area) of 6% was found with maximum values of 30% and minimum values of 0%. CSI values of MESHS from 93% to 36% were computed. 83% was computed as the overall CSI of MESHS. The overall bias of MESHS was smaller than 1.

Table 4.1: Scoring parameters of 2009 for POH and MESHS.

Date	number of ground-truth reports	POD POH	FAR POH	CSI POH	bias POH	POD MESHS	FAR MESHS	CSI MESHS	bias MESHS
12.05.2009	28	0.96	0.39	0.59	1.59	0.86	0.00	0.86	0.86
21.05.2009	46	1.00	0.21	0.79	1.27	0.93	0.00	0.93	0.93
26.05.2009	389	0.99	0.09	0.89	1.09	0.90	0.02	0.89	0.92
06.06.2009	50	0.90	0.41	0.55	1.52	0.36	0.02	0.36	0.37
22.06.2009	104	0.85	0.15	0.74	0.99	0.83	0.30	0.61	1.17
26.06.2009	47	0.91	0.28	0.67	1.28	0.49	0.00	0.49	0.49
14.07.2009	148	0.99	0.39	0.61	1.62	0.85	0.22	0.69	1.09
17.07.2009	148	0.99	0.13	0.86	1.13	0.81	0.00	0.81	0.81
23.07.2009	701	0.99	0.11	0.89	1.11	0.94	0.09	0.87	1.03
02.08.2009	33	0.97	0.33	0.66	1.44	0.76	0.14	0.67	0.89
25.08.2009	37	0.97	0.08	0.89	1.06	0.78	0.00	0.78	0.78
Overall 2009	1731	0.97	0.19	0.79	1.21	0.87	0.06	0.83	0.92

4.1.2. Verification scores 2010

Table 4.2 shows the calculated POD, FAR, CSI and bias scores for all 10 considered hail events of 2010. On two dates (July 3th, July 29th) no false alarm area (FAA) was determined due to the fact that the MESHS area was too small to make an objective verification of the false alarm. An overall POD of POH (weighted with the number of ground-truth reports) of 95% was found with maximum values of 99% and minimum values of 90%. An overall FAR of POH (weighted with the considered area) of 19% was found with maximum values of 41% and minimum values of 6%. The CSI of POH shows values from 90% to 57%. An overall CSI of POH of 78% was calculated. The overall bias of POH was for all events (excepted June 6th) greater than 1. An overall POD of MESHS (weighted with the number of ground-truth reports) of 74% was found with maximum values of 95% and minimum values of 7%. An overall FAR of MESHS (weighted with the considered area) of 6% was found with maximum values of 28% and minimum values of 0%. CSI values of MESHS from 95% to 57% were computed. 71 % was calculated as the overall CSI of MESHS. The overall bias of MESHS was smaller.

Table 4.2: Scoring values of POD, FAR, CSI and bias for 10 events of 2010.

Date	number of ground-truth report	POD POH	FAR POH	CSI POH	bias POH	POD MESHS	FAR MESHS	CSI MESHS	bias MESHS
11.05.2010	153	0.96	0.06	0.90	1.03	0.90	0.09	0.83	0.98
06.06.2010	40	0.98	0.25	0.74	1.29	0.75	0.15	0.66	0.89
08.06.2010	31	0.90	0.08	0.84	0.98	0.87	0.10	0.80	0.96
03.07.2010	81	0.90	0.16	0.77	1.08	0.62	n.a.	n.a.	n.a.
10.07.2010	83	0.98	0.15	0.84	1.14	0.88	0.05	0.84	0.93
12.07.2010	63	0.92	0.14	0.80	1.07	0.75	0.00	0.75	0.75
14.07.2010	42	0.98	0.18	0.80	1.20	0.95	0.00	0.95	0.95
22.07.2010	62	0.98	0.19	0.80	1.21	0.87	0.00	0.87	0.87
29.07.2010	70	0.99	0.26	0.73	1.33	0.07	n.a.	n.a.	n.a.
01.08.2010	37	0.95	0.41	0.57	1.61	0.73	0.28	0.57	1.01
Overall 2010	662	0.95	0.19	0.78	1.18	0.74	0.06	0.71	0.79

4.1.3. Verification scores 2011

Table 4.3 shows the calculated POD for all 32 considered hail events of 2011. FAR, CSI and bias were not calculated due to the small number of ground-truth observations of 2011. For 2011 an overall POD of POH of 94% was found with maximum values of 100% and minimum values with 0%. For the POD of MESHS maximum values of 100% and minimum values of 0 % were found as well. The same range was found for HAIL. A 77% overall POD of MESHS was calculated. The overall POD of HAIL was 84%. Events of POH, MESHS and HAIL with 0% probability mean that the ground-truth reports were not covered by the corresponding signal of the POH, MESHS or HAIL product. The radar-based hail detection algorithms underestimated the occurrence of hail at those locations. But only the overall POD, MESHS and HAIL can be used in terms of a reliable declaration. Interpretations about single hail events are not valid, except of July 07 and July 12, 2011, due to the small number of observations. It is more likely that a single observation is missing due to the algorithms than events with higher numbers of ground-truth reports. This is in the nature of things. Therefore, further investigations about the single events are not useful.

4.1.4. Overall verification scores

Overall verifications scores of the three years 2009, 2010 and 2011 are shown in table 4.4. Overall POD of POH of 97% was found (weighted with the number of ground-truth hail observations). FAR of POH (weighted with the considered areas) of 19% and CSI of POH of 79% were found. The single values of all three years are more or less similar. The bias was computed as 1.20 and is greater as 1.

An overall POD of MESHS score of 83% was calculated. POD was calculated as the weighted average of all ground-truth hail observations. For 2010 and 2011 lower POD of MESHS were found. Because of the higher number of ground-truth observations of 2009 the overall POD of MESHS is closer to this certain value. The overall FAR of MESHS (weighted with the considered areas) was computed as 6%. Overall CSI of MESHS was found as 79% and the overall bias of MESHS as 89%. The bias of MESHS of 2009 was closer to 1 then the bias of MESHS of 2010.

For the HAIL product POD of 2011 was only calculated. A value of 84% was found.

Table 4.3: PODs of POH, MESHS and HAIL of 2011.

Date	number of ground-truth report	POD POH	POD MESHS	POD HAIL
15.05.2011	3	0.67	0.00	0.00
22.05.2011	2	1.00	1.00	1.00
26.05.2011	8	1.00	0.63	0.88
27.05.2011	4	0.50	0.00	0.00
05.06.2011	1	1.00	1.00	1.00
06.06.2011	2	1.00	0.00	0.50
16.06.2011	1	1.00	0.00	0.00
21.06.2011	4	1.00	0.75	0.75
22.06.2011	11	0.91	0.36	0.82
28.06.2011	1	0.00	0.00	0.00
29.06.2011	3	1.00	0.67	0.67
07.07.2011	36	1.00	0.86	0.94
09.07.2011	2	1.00	1.00	1.00
10.07.2011	5	1.00	0.50	0.50
12.07.2011	53	1.00	0.80	0.60
19.07.2011	1	1.00	1.00	0.98
27.07.2011	1	1.00	1.00	1.00
03.08.2011	5	1.00	1.00	1.00
08.08.2011	3	0.00	0.60	0.80
18.08.2011	3	1.00	0.00	0.00
19.08.2011	1	0.00	1.00	1.00
23.08.2011	7	1.00	0.00	0.00
24.08.2011	13	1.00	0.71	0.86
25.08.2011	2	1.00	1.00	1.00
26.08.2011	7	1.00	0.50	1.00
27.08.2011	1	1.00	0.57	0.86
02.09.2011	2	1.00	0.00	0.00
04.09.2011	1	1.00	1.00	1.00
05.09.2011	2	0.00	1.00	1.00
11.09.2011	8	1.00	0.00	0.00
12.09.2011	1	0.00	1.00	1.00
16.09.2011	2	1.00	1.00	1.00
Overall 2011	196	0.94	0.77	0.84

Table 4.4: POD of POH, MESHS and Hail for 2009, 2010 and 2011 as well as FAR and CSI for 2009 and 2010. The overall values are weighted values according to the number of observations.

Year	number of ground-truth report	POD POH	FAR POH	CSI POH	bias POH	POD MESHS	FAR MESHS	CSI MESHS	bias MESHS	POD HAIL
2009	1731	0.97	0.19	0.79	1.21	0.87	0.06	0.83	0.92	n.a.
2010	662	0.95	0.19	0.78	1.18	0.74	0.06	0.71	0.79	n.a.
2011	196	0.94	n.a.	n.a.	n.a.	0.77	n.a.	n.a.	n.a.	0.84
Overall	2589	0.97	0.19	0.79	1.20	0.83	0.06	0.79	0.89	0.84

4.2. MESHS

Self-collected ground-truth hail reports were used in order to verify the correlation of MESHS with real observed hail diameters. Figure 4.1 shows a scatter plot of the detected $MESHS_{median}$ values and maximum observed hail size. $MESHS_{median}$ values are the medians of each 3x3 verification matrix. In total 122 different ground-truth reports were used. Some of them were plotted as one single cross due to the same values. A correlation value (r) of 45.01% was found. Figure 4.2 shows the correlation of $MESHS_{max}$ and maximum observed hail diameters. $MESHS_{max}$ is the maximum detected MESHS value within each 3x3 verification matrix. A slightly higher r of 47.81% was found. The same was computed with MESHS values which were greater than zero (values which were observed by the finders). For $MESHS_{median}$ a correlation of 30.85% was found. For $MESHS_{max}$ a correlation of 37.47% was found. These figures are in the appendix (7.1; 7.2). Figure 4.3 shows the deviation of MESHS (cm) from the maximum observed hail size diameters. Hailstone diameters up to 4.5 cm were overestimated with the MESHS algorithm in general, whereas greater hailstone diameters were underestimated. The crosses with negative deviations from 0.4-2.5cm are missing events. The MESHS algorithm did not detect hail at those locations.

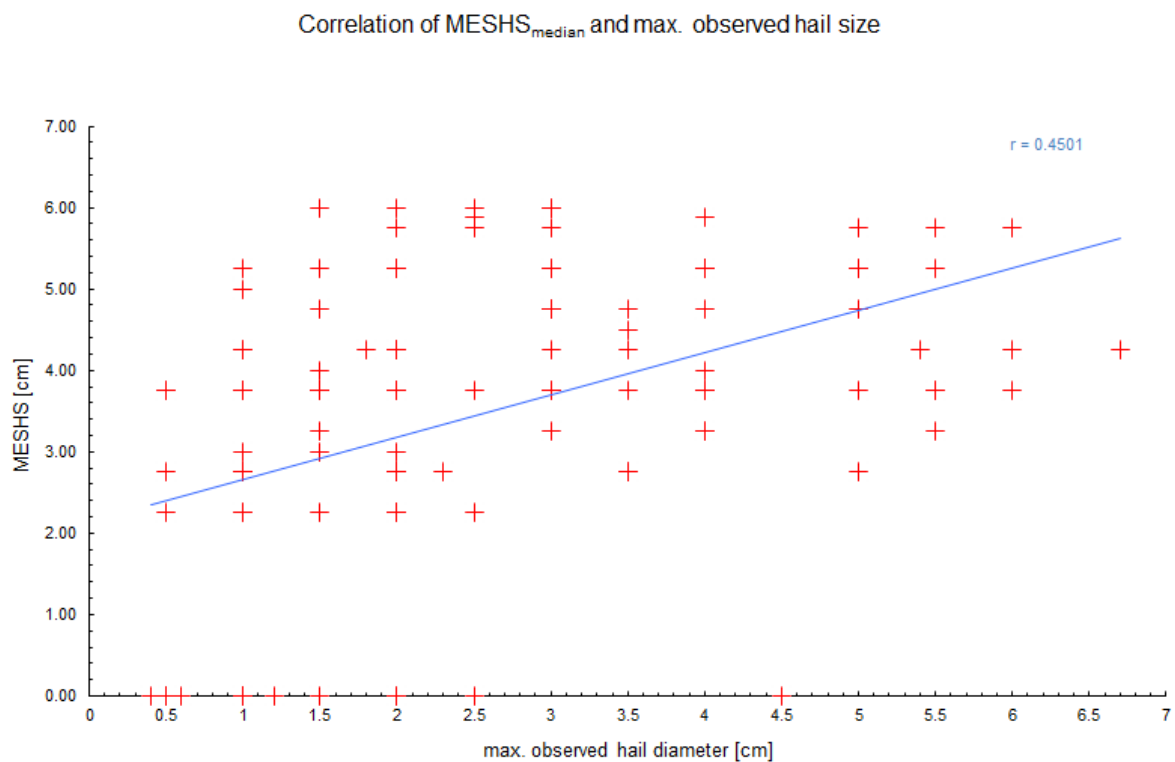


Figure 4.1: Correlation of $MESHS_{median}$ values and maximum observed hail diameter for the year 2011 (red crosses). r is the coefficient of correlation. The blue line shows the line of the computed linear regression. On the x-axis maximum observed hail diameters are shown in cm. The y-axis shows the corresponding MESHS values in cm.

Correlation of MESH_S_{max} and max. observed hail size

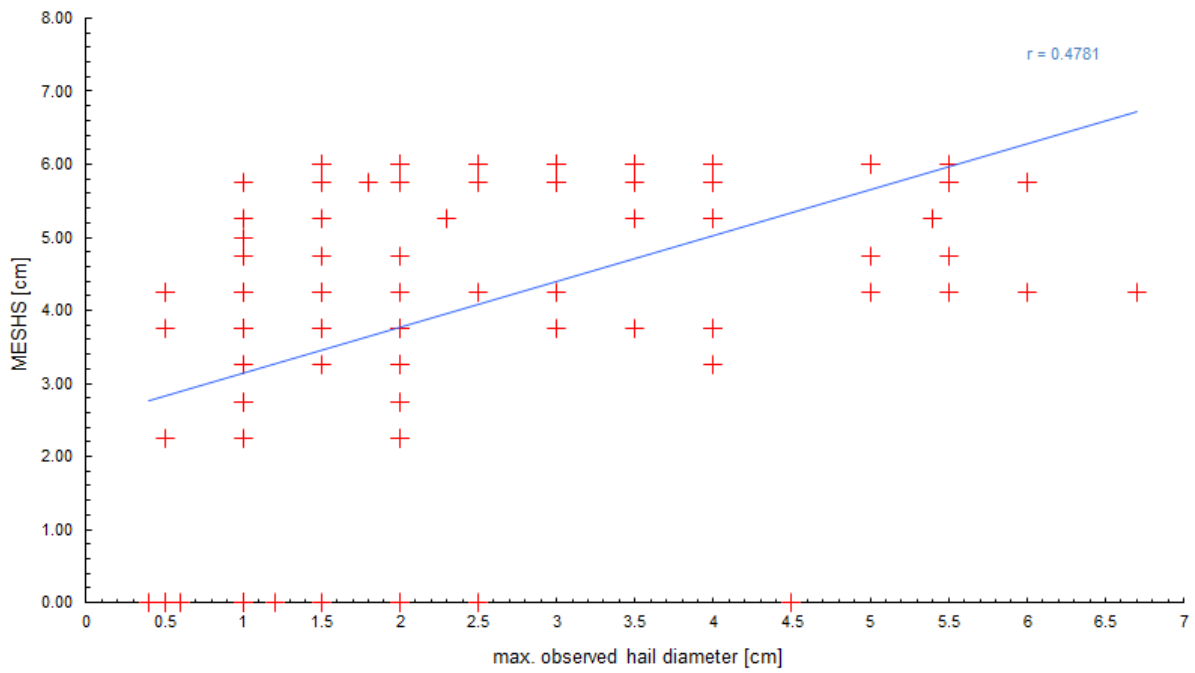


Figure 4.2: Correlation of MESH_S_{max} values and maximum observed hail diameter for the year 2011 (red crosses). *r* is the coefficient of correlation. The blue line shows the line of the computed linear regression. On the x-axis maximum observed hail diameters are shown in cm. The y-axis shows the corresponding MESH_S values in cm.

Deviation of MESH_S_{median} in cm
ordered by hail size

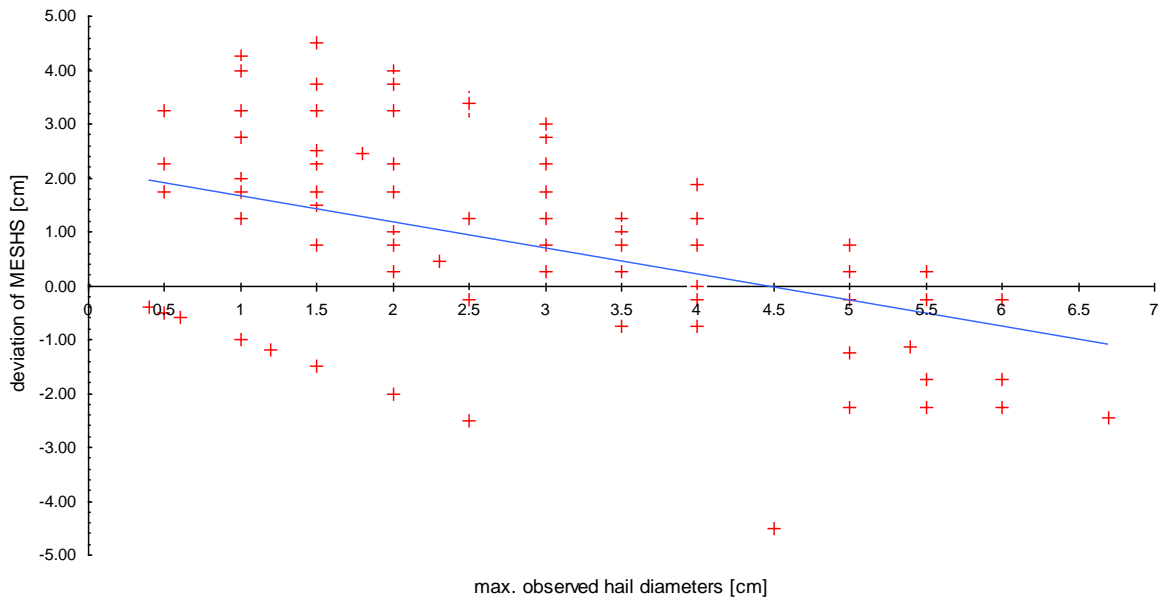


Figure 4.3: Over- and underestimation of hailstone diameters due to the MESH_S algorithm. Red crosses are the deviation of MESH_S values (cm) from the maximum observed hail diameters. The blue line shows the linear trend. The red crosses with negative deviation from 0.4-2.5cm are missing events.

4.3. POH

Specific calculations of the goodness of POH were difficult to make. In terms of probabilities a simple calculation was executed. Ground-truth reports showed where hail was occurred. The POH algorithm should detect a 100% probability. Therefore, the deviation of POH values from 100% were calculated and plotted with its corresponding hail size (figure 4.4). Hail diameters up to 2.5 cm had a greater spread in terms of deviation (dashed blue line). Without the outlier at 4.5 cm only hailstones smaller than 2.5 cm shows probabilities smaller than 90%. The smaller the probability of POH, the higher is the chance that POH misses the hail event.

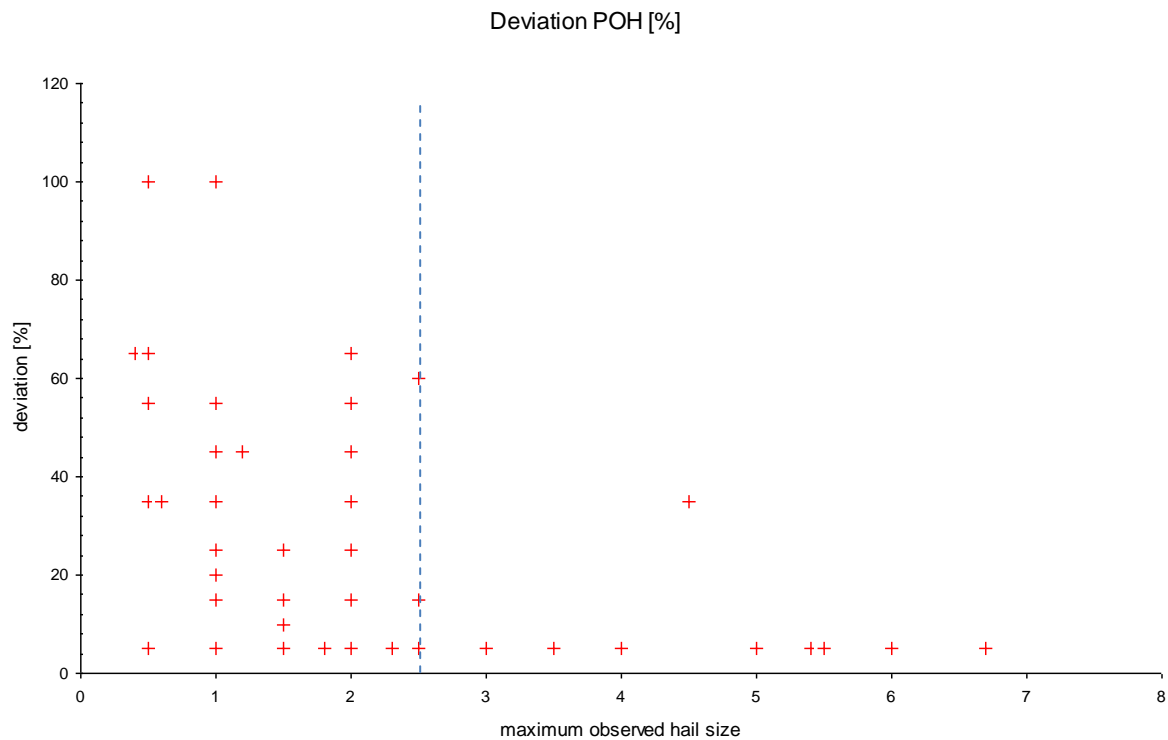


Figure 4.4: Deviation of POH values from 100% probability of hail. Small hail diameters show greater variances than greater hail diameters. The dashed blue line shows the limit in terms of deviation of POH.

4.4. Climatology

For the year 2009 and 2010 enough data were available in order to determine in which months the most hail events occurred. The month with the highest number of hail events occurred in both years on July. During the period from May until July the number of hail events increased continuously. After July the number decreased rapidly. During the hail season 2009 much more days with hail were counted. Especially for May and June 2009 high numbers were counted (figure 4.5 and figure 4.6). More information about Swiss hail climatology can be found in Willemse (1995).

Number of hail days after months 2009

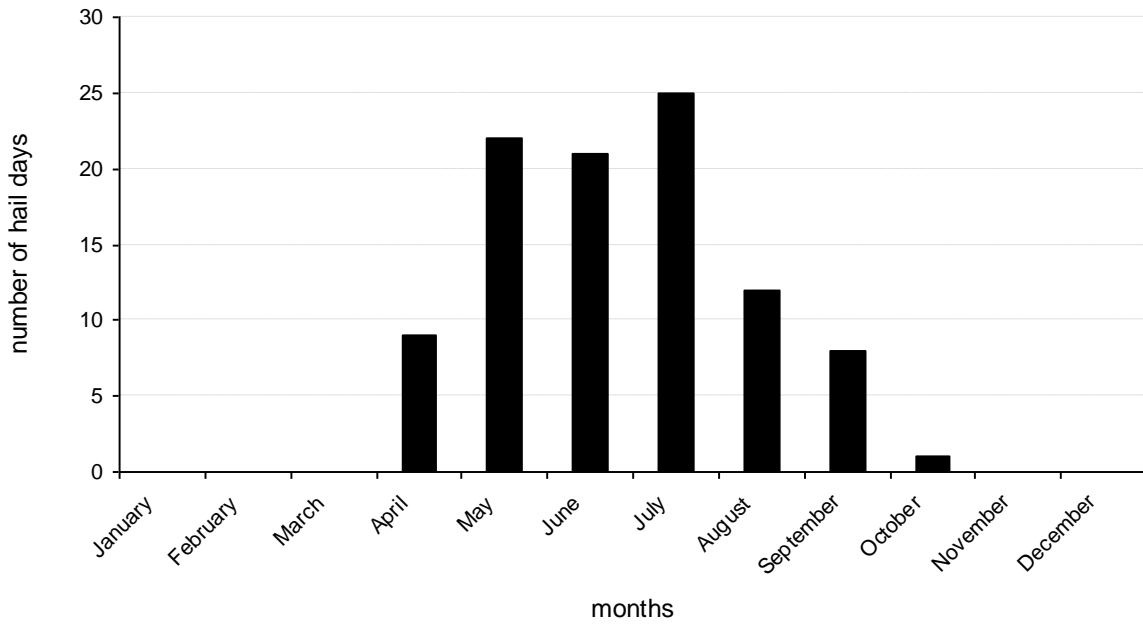


Figure 4.5: Number of hail days for the year 2009. The figures were computed with data of the Swiss hail insurance.

Number of hail days after months 2010

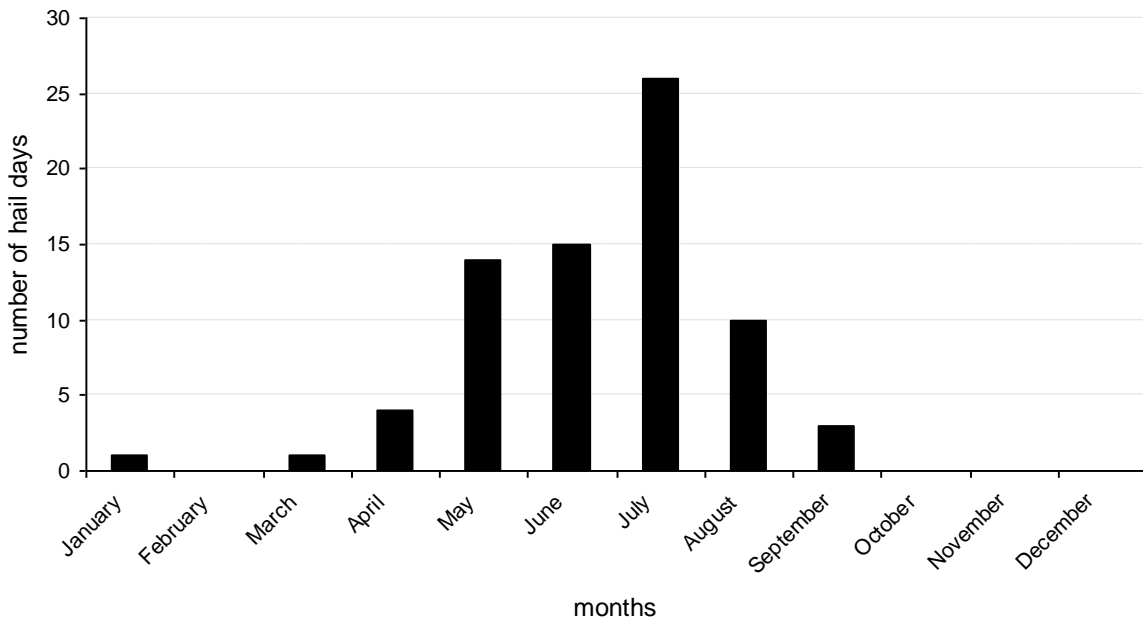


Figure 4.6: Number of hail days for the year 2010. The figures were computed with data of the Swiss hail insurance.

4.4.1 Radar-based hail climatology

Google Earth allows plotting all available radar-based hail detection products of any kind of combination as single layers. As mentioned in the previous chapters, the visualized layers in Google Earth are usually transparent and colors are only visible where the radar algorithms calculated hail. For climatological-based hail maps different layers can be overlaid. The output then shows for each 2x2 km pixel whether there was hail calculated with the corresponding hail detection algorithm and for the corresponding time period or not. Pixels where no hail was calculated within a certain time period are still transparent. Otherwise, if there is a colored pixel at least once hail was calculated. The figure 4.7 shows overlaid MESHS layers for Mai-September 2009-2011. Additional figures can be found in the appendix (7.3). The yellow line is the Swiss border as well as borders of surrounding countries. The dark lines are lake and river contours.

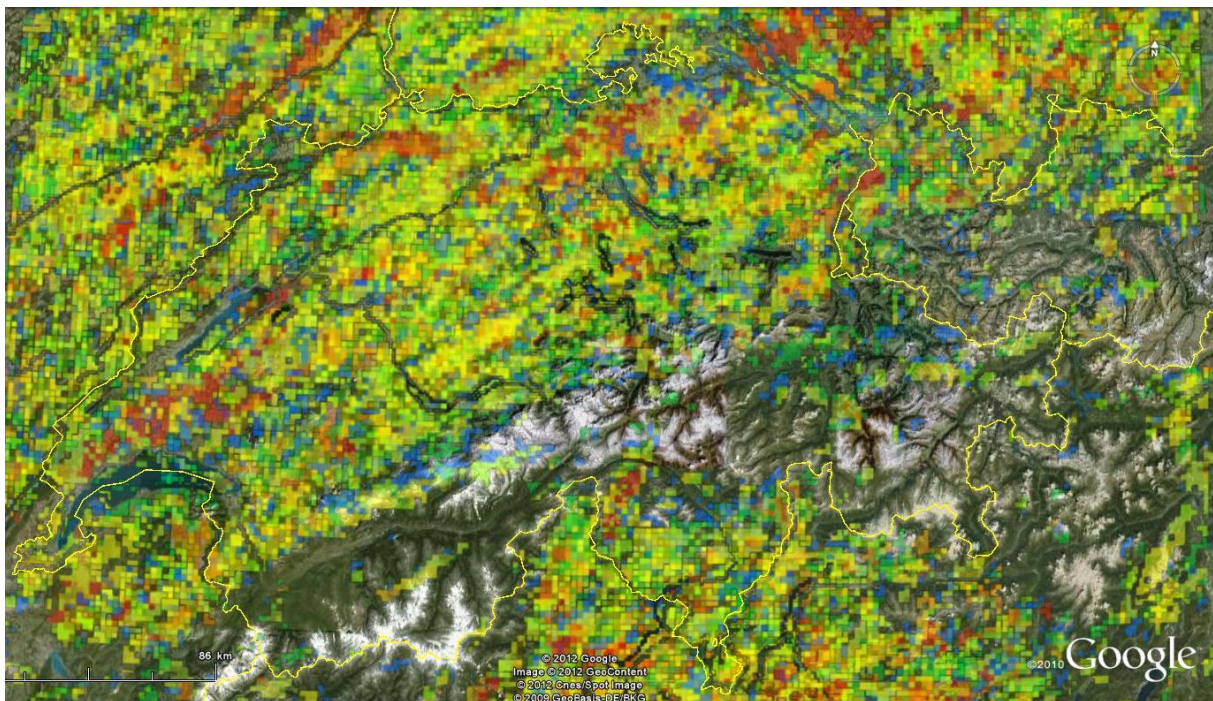


Figure 4.7: MESHS pixels of the hail seasons (May – September) 2009, 2010 and 2011 in colors. The yellow lines are international borders. Black lines are river and lake contours.

Hail affects huge parts of Switzerland and no area can be save of it. Over the three seasons time period hail was detected for nearly every pixel except the alpine region (4.7). That could have meteorological reasons as well as technical reasons due to radar scan properties. The latter can be seen on the visibility map of the Swiss radar composite (7.10). The radar visibility is limited over alpine region. Weak convection over valleys might be not seen. However, lightning climatology maps confirm in general the relatively lower occurrence of thunderstorms in the interior alpine valleys (not shown).

The difference in terms of the area with detected hail between POH and MESHS is impressive (figures 7.3 and 7.4). It shows again the advantages of the MESHS product in order to use it for forecasts. POH shows nearly for every single pixel the occurrence of hail for the hail season 2009 whereas in MESHS still areas without any hail signal can be recognized. The same is valid for the year 2010 (figures 7.5 and 7.6). MESHS underestimates the occurrence of hail but with its low FAR the determination of hail is reliable.

7.9 shows HAIL pixels of the hail season 2011. The main hail areas were detected in visibility areas between 0-1900 m (white areas in figure 7.10) whereas over Valais and Grisons no hail was detected. That is in agreement with the observations in the POH and MESHS outputs.

The layer-based analysis allows a simple and quick visualization of the radar-based hail detection products for longer time periods. All products are available in operational use and the further computation applications have been created. However, the introduced findings are just preliminary results. The whole radar-based hail climatology with POH, MESHS and the HAIL algorithm need more research.

4.5. POH 4th generation

The new radar on Monte Lema and La Dôle made it possible to implement first experimental hail detection products. The POH product of the fourth generation (POH 4th) was analyzed to recognize obvious improvements in terms of hail detection, due to adaptations of the algorithm. Two cases (24.08.2011 and 11.09.2011) were animated in Google Earth. In different other cases, better detection properties were observed. Small scale phenomena were better detected due to better resolution and adaptations of probability thresholds.

A good example is given in figure 4.8, where a small thunderstorm cell crossed the region of the Lake Constance on the August 08, 2011. On the left hand side no hail signal was observed at 08.35 UTC. On the right hand side, some pixels with values up to 20% were detected. In fact, graupel with diameter of 0.5 cm was observed.

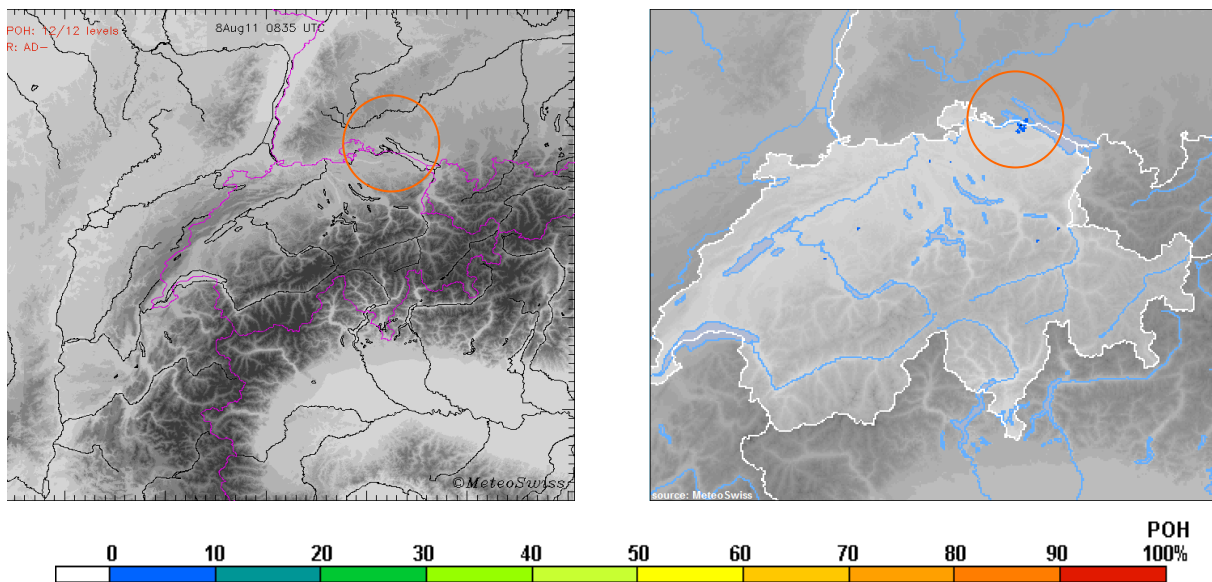


Figure 4.8: Comparison of POH products of the old generation (left) and new generation (right) on July 03 2011. On the output of the new generation (right) hail probabilities up to 20% were detected (orange circle), while on the old output (left) no hail probability was detected (orange circle).

5. Conclusion and recommendations

Three different radar-based hail detection algorithms of MeteoSwiss's radar network have been verified. The recalculations of the daily integrated hail detection products improved the size of the archive. With the collection of ground-truth hail observations from different sources it has been shown that the combination of these sources is possible and useful. This study further made the first step in creating a ground-truth hail observation data base for Switzerland (SHVDB) using the Internet as a source. These sources were combined with more traditional data such as insurance loss data. The different sources showed the same patterns in terms of hailstorms.

In total, 11981 single ground-truth hail reports were used for this verification project. Because of the higher resolution of the insurance loss reports, these had to be summarized at municipality level. Therefore, 3644 reports with a resolution on commune level have finally been used. Approximately 3500 ground-truth hail reports were visualized in Google Earth. Other comprehensive studies (e.g. Ortega et al., 2009; Wilson et al., 2009) used up to 3921 different ground-truth data. Studies like Kessinger et al. (1995) or Witt et al. (1998) used 237 and 107 respectively. Overall, the size of the data base is in line with other studies. The resolution is high, especially in comparison with the data bases of North-American studies, when data were collected for a much wider area.

For the hail season 2011 ground-truth hail observations had to be collected to determine the Goodness of MESHS and POH. With a few exceptions, ground-truth hail reports may be found for nearly every detected hail event. In total 196 reports were collected for the year 2011, and a huge number of observations also include information about the hail size.

Scoring parameters such as Probability of Detection (POD) and False Alarm Rate (FAR) for hail swaths have been calculated as well as critical success index (CSI) and the corresponding bias. An overall POD of 0.97 was found for the POH algorithm. This agrees with other studies (e.g. Brimelow et al., 2006) which have found a 0.93 POD score. The FAR was calculated as the ratio between POH covered areas with ground-truth observation and POH covered areas without ground-truth observations. For POH a FAR of 0.2 was computed. For MESHS and HAIL overall PODs of 0.83 and 0.84 were found. For the HAIL algorithm the POD was only determined with ground-truth observations of 2011. An overall FAR of 0.06 was found for MESHS.

High CSIs were found as well. The overall CSI of POH was computed as 0.78 and as 0.79 for MESHS. Compared with literature, these values are high and emphasize the quality of MeteoSwiss's radar-based hail detection products. The biases show that POH overestimates the occurrence of hail in general, while MESHS underestimates the occurrence of hail. The analysis of POH has shown that probabilities smaller than 90% were observed for hailstone diameters smaller than 2.5 cm.

The MESHS algorithm looks more robust in terms of FAR but has a lower probability of detection. The limitations of MESHS are clear: the study have suggested that correlations between MESHS values and ground-truth hail size data are small. Statements about the hail size on the ground are afflicted

with huge uncertainties. Notwithstanding its limitations, this study emphasizes that the MESHS algorithm is very useful to detect hail in a solid and robust manner. It is a useful tool in detecting severe hail cells and possibly useful for related applications such as warnings, nowcasts and simple climatology.

The daily integrated POH, MESHS and HAIL products give an overview of the current situation. Areas, which were affected by a hailstorm, can be identified quite easily. The study has shown that all three radar-based hail detection algorithms are useful in detecting hail, with better results in terms of the CSI scoring parameter for POH and MESHS. Although Switzerland is a mountainous country, the radar network and its algorithm work well in comparison with other studies. For some cases, the algorithms detected even small scale hail events (figure 7.11, 7.12). All radar outputs and ground-truth hail observations were saved in one single file (Hail Switzerland 2009, 2010, 2011.kmz) and can be used for further applications.

Internet and social media as well as traditional media are valuable sources for verifying radar-based hail detection algorithms. Therefore, collecting of weather-related data, and ground-truth hail observation reports especially, should be pursued. These new possibilities will be increasingly important in future. It is important not to miss the chance.

This study has gone in a new direction in doing verifications of radar-based hail products in the alpine and pre-alpine region. New possibilities in collecting ground-truth hail data, in visualization and in georeferencing have been applied. In agreement with recent studies (e.g. Wilson et al., 2009; Ortega et al., 2009), Google Earth has been used to visualize ground-truth hail observations, radar-based hail detection algorithm outputs, as well as hail swaths. It visualizes geo data in a fast and user-friendly way. The program hailge_operational.sh calculates Google Earth's KML files for the three products POH, MESHS and HAIL. Insurers and all kinds of media ask for information and explanations why and where a severe hailstorm was occurred immediately. Hail swaths visualization in Google Earth could be a new and impressive method.

In order to gain more statistically tested results, the collected ground-truth data and insurance loss data could be analyzed with consideration of different statistical weights of the single observations. The stage of plant growth can be considered for more detailed analysis as well. Google Earth may be used for further climatology and as a powerful visualization tool. MESHS and POH may be connected with MeteoSwiss's TRT system (Hering et al., 2004). The direction and the absolute value of the TRT velocity vector may be adapted and used as forecast (nowcast). First semi-quantitative case studies showed good results.

The products are already running operationally, they can be tuned to the need of specific customers.

6. Acknowledgements

I would like to thank the RASA and the MeteoLocarno team for all the support. A special thanks goes to Alessandro Hering for his patience, support and help. Thanks to Marco Gaia for his useful suggestions and the chance to realize this project. Thanks to Clementi Lorenzo, Mandapaka V. Pradeep, Panziera Luca and Sideris Ioannis for their help.

Hansueli Lusti, Imhof Markus, Jordi Martin and Dölf Käppeli are acknowledged for supplying the reports of hail damages of the years 2009 and 2010.

7. Appendix

Table 7.1: Table of all categories for which data were collected and computed

category	Explanation
date	Date
Latitude (WGS84)	geographical latitude in WGS 84
Longitude (WGS84)	geographical longitude in WGS 84
Swissgrid Y	geographical longitude in CH1903
Swissgrid X	geographical latitude in CH1903
location	name of the hailstorm location
Canton	canton of the hailstorm location
source	name of the source(s)
source category	grade of the source
time (MEZ)	time when the hail event occurred
duration (min)	duration of the hail event
hail (1/0) observation	hailstorm occurred (1) or not (0)
maxdiameter (cm)	maximum observed hail size
meandiameter (cm)	mean observed hail size
max. Pixel POH	maximum value of POH within the evaluation matrix
POH (3x3)*	median of POH within the evaluation matrix
pixel POH	number of pixel with a radar information in POH
max. Pixel MESHS	maximum value of MESHS within the evaluation matrix
min.Pixel MESHS	minimum value of MESHS within the evaluation matrix
MESHS (3x3)*	median of MESHS within the evaluation matrix
pixel MESHS	number of pixel with a radar information in MESHS
max. Pixel HAIL	maximum value of HAIL within the evaluation matrix
HAIL (3x3)*	median of HAIL within the evaluation matrix
pixel HAIL	number of pixel with a radar information in HAIL
POH(3x3)**	average of POH within the evaluation matrix
MESHS(3x3)**	average of MESHS within the evaluation matrix
HAIL (3x3)**	average of HAIL within the evaluation matrix
hail (1/0) POH	POH detected hail within evaluation matrix (1) or not (0)
hail (1/0) MESHS	MESHS detected hail within evaluation matrix (1) or not (0)
hail (1/0) HAIL	HAIL detected hail within evaluation matrix (1) or not (0)
calcdetection POH (%)	probability of detection POH within evaluation matrix in %
deviation POH (%)	deviation of POH from 100% probability
calcdetection MESHS (%)	probability of detection MESHS within evaluation matrix in %
diffMESHSmax (cm)	Difference between max. Pixel MESHS and maxdiameter
deviation MESHS (%)	MESHSmmedian minus maxdiameter in cm
calcdetection HAIL (%)	probability of detection HAIL within evaluation matrix in %
type	graupel or hail
additional information	additional information
no max. value	no information about hail size available
> 3 cm	hailstones > 3 cm diameter
< 3 cm	hailstones < 3 cm diameter

7.1. Correlation MESHs

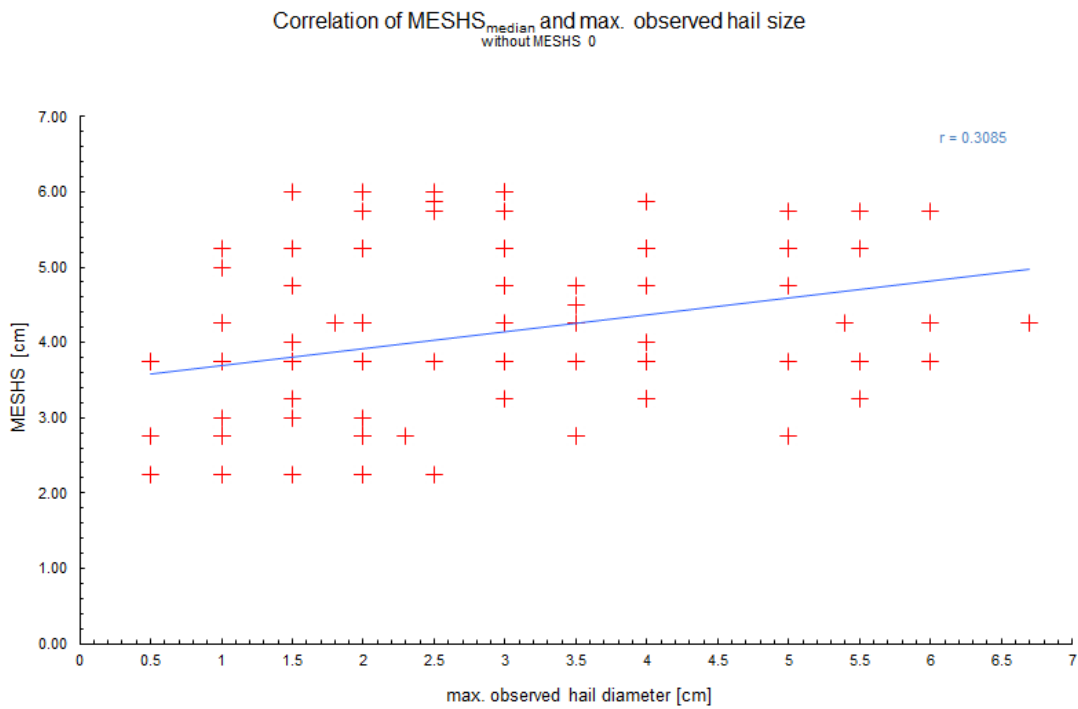


Figure 7.1: Correlation of MESHs_{median} with maximum observed hail sized. So call missing values which were not detected with the MESHs algorithm are not considered.

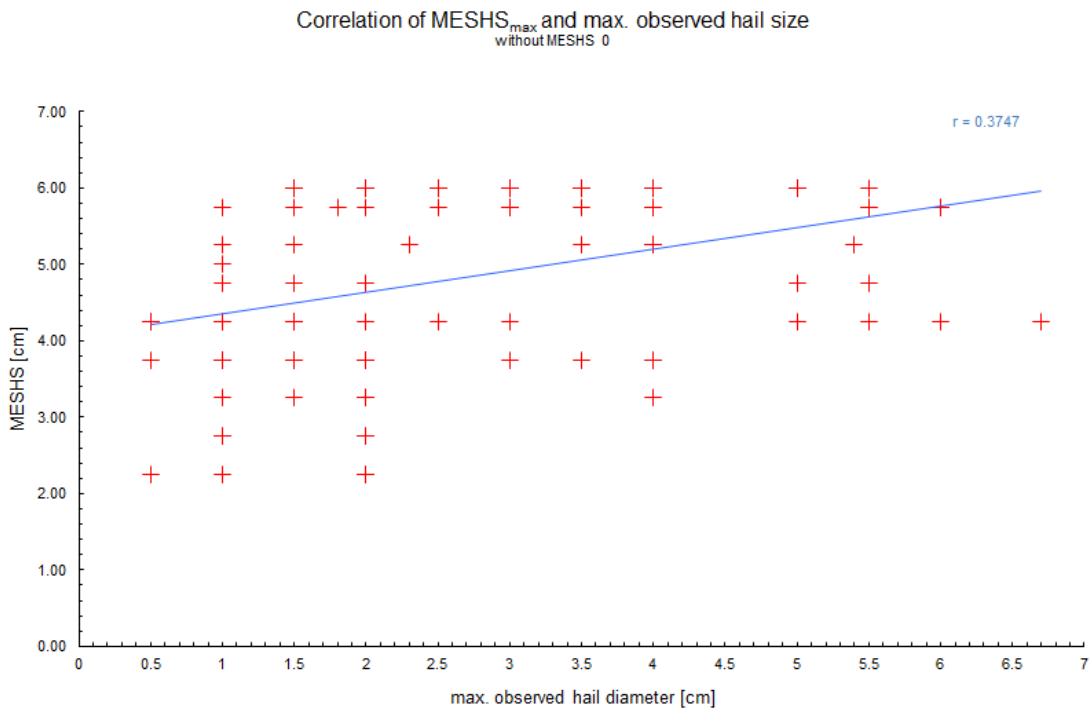


Figure 7.2: Correlation of MESHs_{max} with maximum observed hail sized. So call missing values which were not detected with the MESHs algorithm are not considered.

7.2. Calculations FAR 2009/2010

Table 7.4: Calculations of FAR 2009.

Date	area POH [km ²]	FAA POH [km ²]	FAR POH	area MESHs [km ²]	FAA MESHs [km ²]	FAR MESHs	Missed ground-truth obs. POH	Missed ground-truth obs. MESHs	total of ground-truth observations	POD POH	POD MESHs
12.05	1301	513	0.39	251.5	0	0.00	1	4	28	0.96	0.86
21.05	2006	427.9	0.21	414.4	0	0.00	0	3	46	1.00	0.93
26.05	7623	723.6	0.09	3518.6	57.8	0.02	5	37	389	0.99	0.90
06.06	1486.9	607.9	0.41	270.1	4.93	0.02	5	32	50	0.90	0.36
22.06	1227.3	181.3	0.15	110.6	32.7	0.30	16	18	104	0.85	0.83
26.06	1008	285.9	0.28	98.6	0	0.00	4	24	47	0.91	0.49
14.07	5268	2050.7	0.39	760.5	166.9	0.22	2	22	148	0.99	0.85
17.07	4241	533.4	0.13	866	0	0.00	2	28	148	0.99	0.81
23.07	7956	850	0.11	3844	328	0.09	7	41	701	0.99	0.94
02.08	1441.8	470	0.33	186.7	27	0.14	1	8	33	0.97	0.76
25.08	1042.6	87.3	0.08	271	0	0.00	1	8	37	0.97	0.78
Overall	34601.6	6731	0.19	10592	617.33	0.06	44	225	1731	0.97	0.87

Table 7.5: Calculations FAR 2010.

Date	area POH [km ²]	FAA POH [km ²]	FAR POH	area MESHs [km ²]	FAA MESHs [km ²]	FAR MESHs	Missed ground-truth obs. POH	Missed ground-truth obs. MESHs	total of ground-truth observations	POD POH	POD MESHs
11.05	2742	175	0.06	1380	120	0.09	6	16	153	0.96	0.90
06.06	1703.7	418.3	0.25	309.5	47.4	0.15	1	10	40	0.98	0.75
08.06	722	57	0.08	347	33.5	0.10	3	4	31	0.90	0.87
03.07	1792.5	292.9	0.16	n.a.	n.a.	n.a.	8	31	81	0.90	0.62
10.07	2106	306.6	0.15	514.1	27.6	0.05	2	10	83	0.98	0.88
12.07	1512	210	0.14	454	0	0.00	5	16	63	0.92	0.75
14.07	2761.6	509.6	0.18	456.4	0	0.00	1	2	42	0.98	0.95
22.07	2291	424	0.19	1002	0	0.00	1	8	62	0.98	0.87
29.07	2450	634	0.26	n.a.	n.a.	n.a.	1	65	70	0.99	0.07
01.08	2101.5	864.9	0.41	220.1	61.1	0.28	2	10	37	0.95	0.73
Overall	20182.3	3892.3	0.19	4683.1	289.6	0.06	30	172	662	0.95	0.74

7.3. Radar based hail climatology

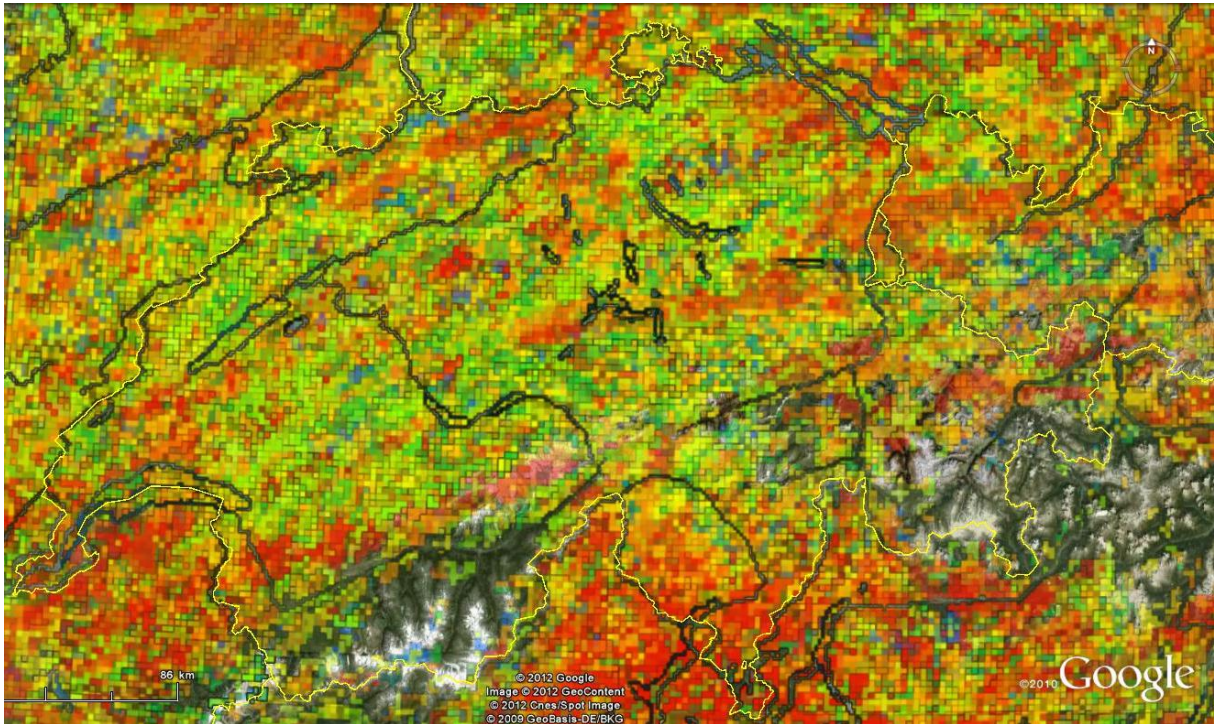


Figure 7.3: POH pixels of the hail season (May – September) 2009 in colors. The yellow lines are international borders.

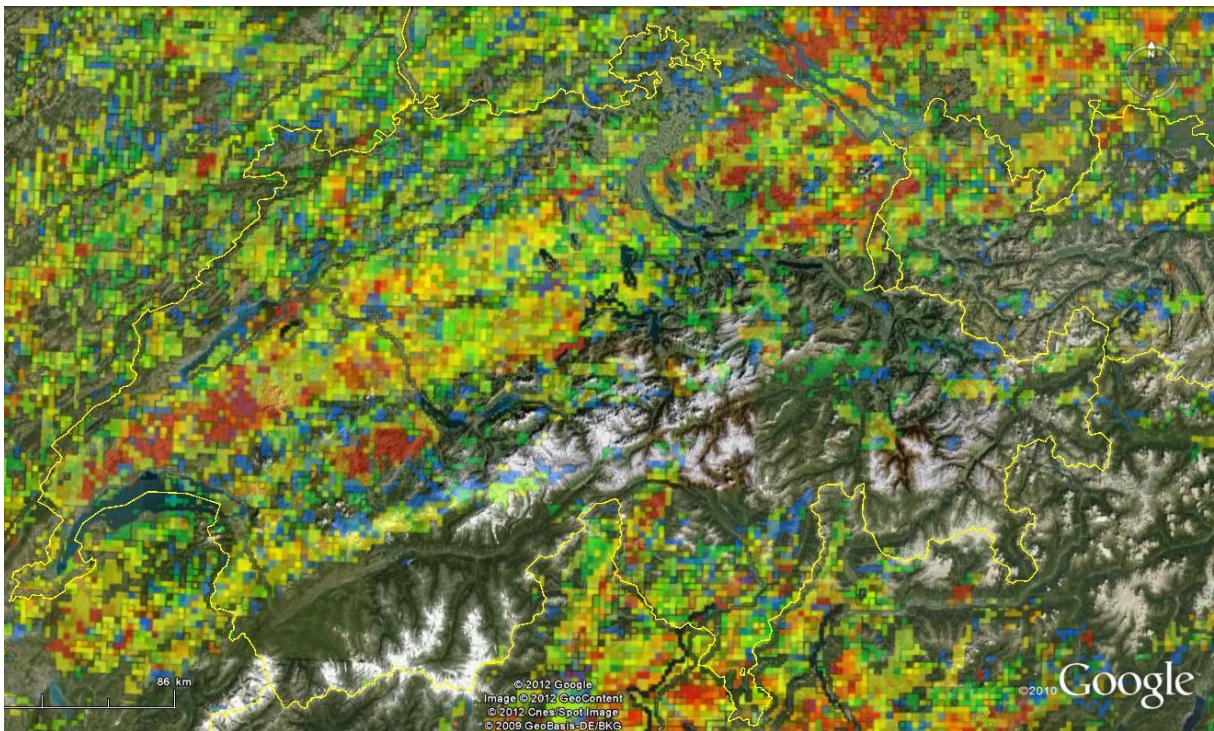


Figure 7.4: MESHS pixels of the hail season (May – September) 2009 in colors. The yellow lines are international borders.

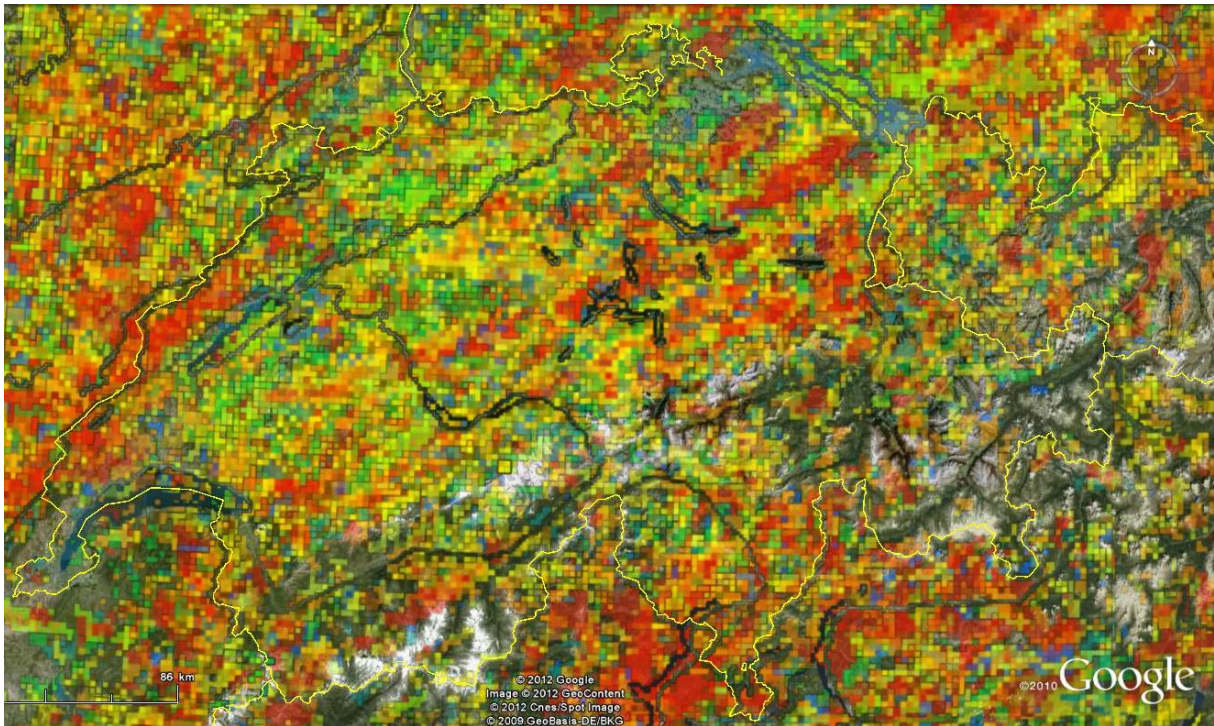


Figure 7.5: POH pixels of the hail season (May – September) 2010 in colors. The yellow lines are international borders.

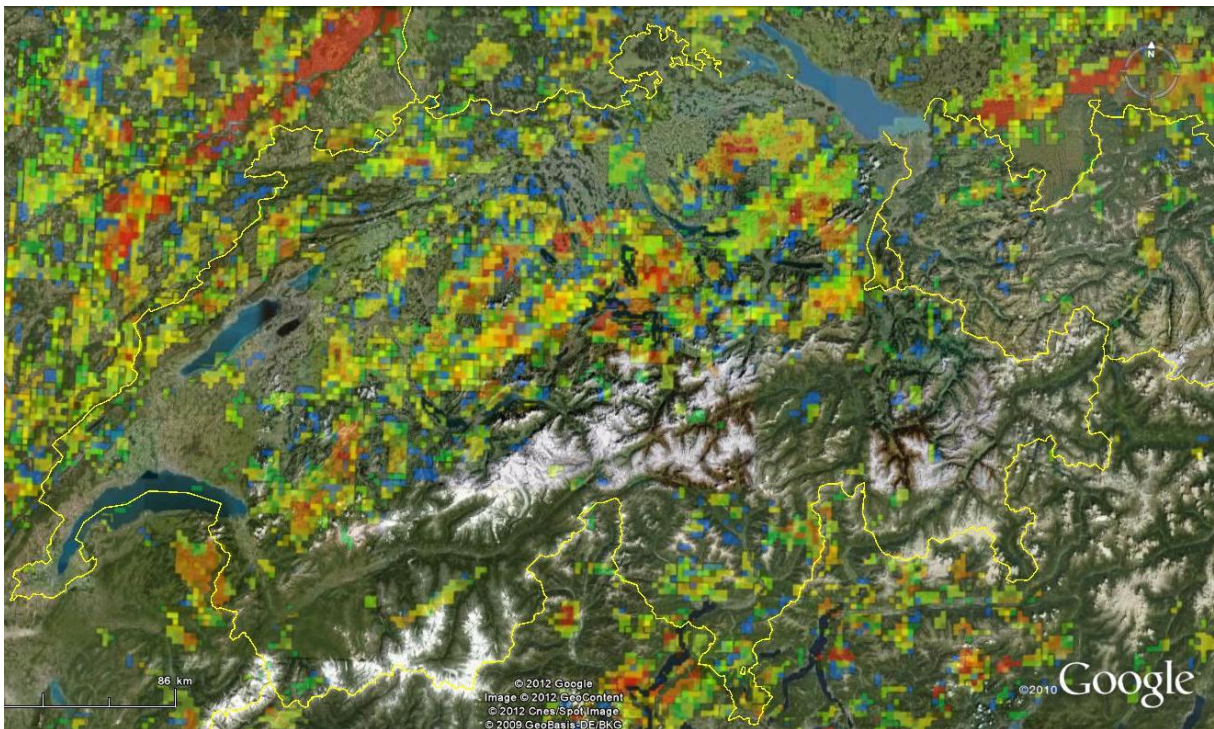


Figure 7.6: MESHS pixels of the hail season (May – September) 2010 in colors. The yellow lines are international borders.

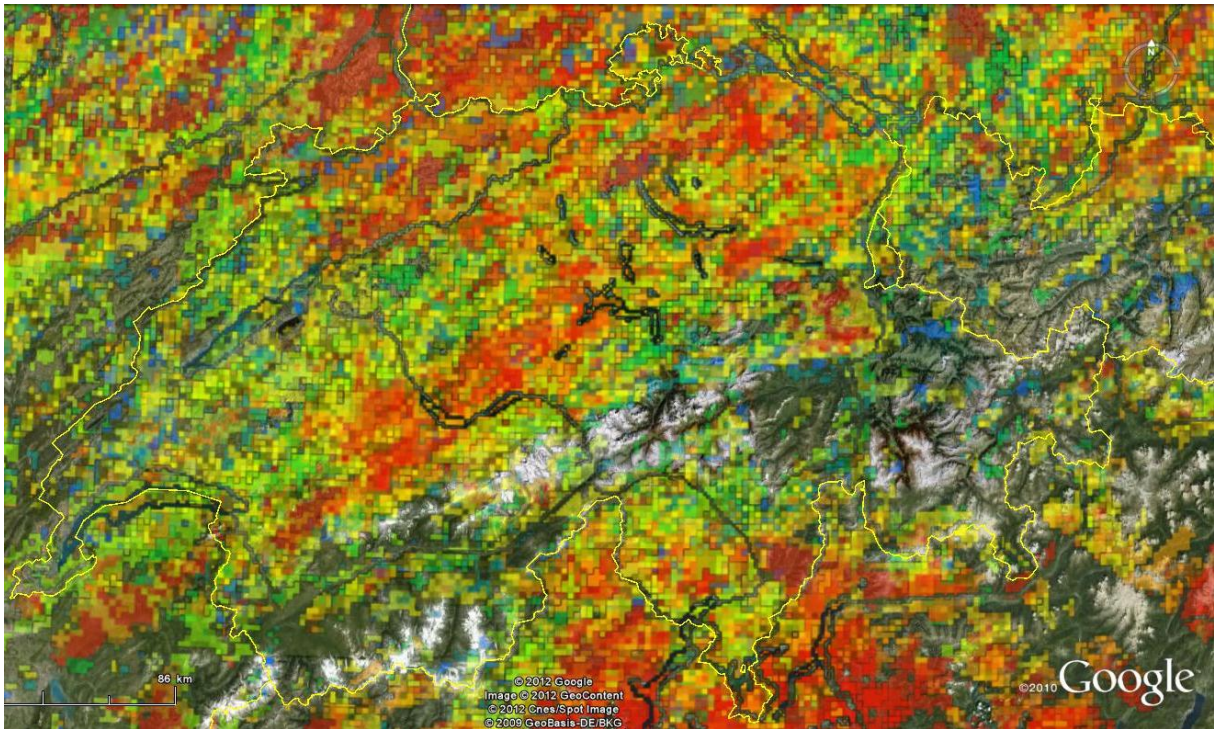


Figure 7.7: POH pixels of the hail season (May – September) 2011 in colors. The yellow lines are international borders.

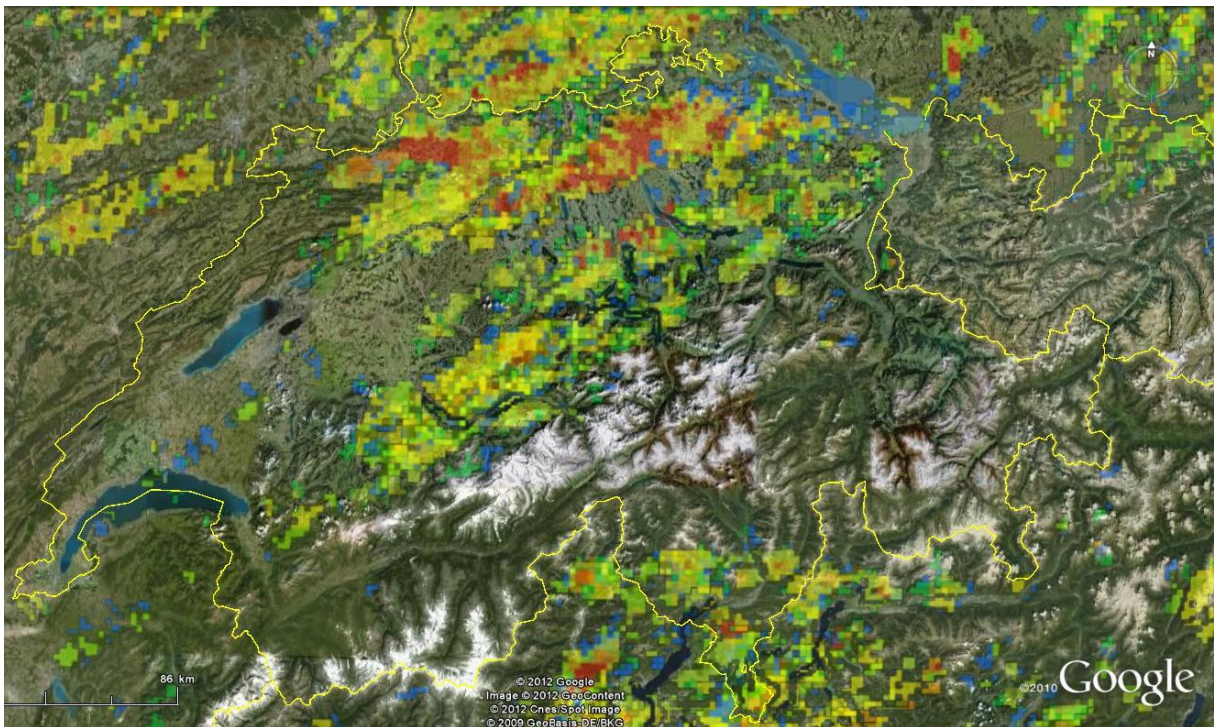


Figure 7.8: MESHS pixels of the hail season (May – September) 2011 in colors. The yellow lines are international borders.

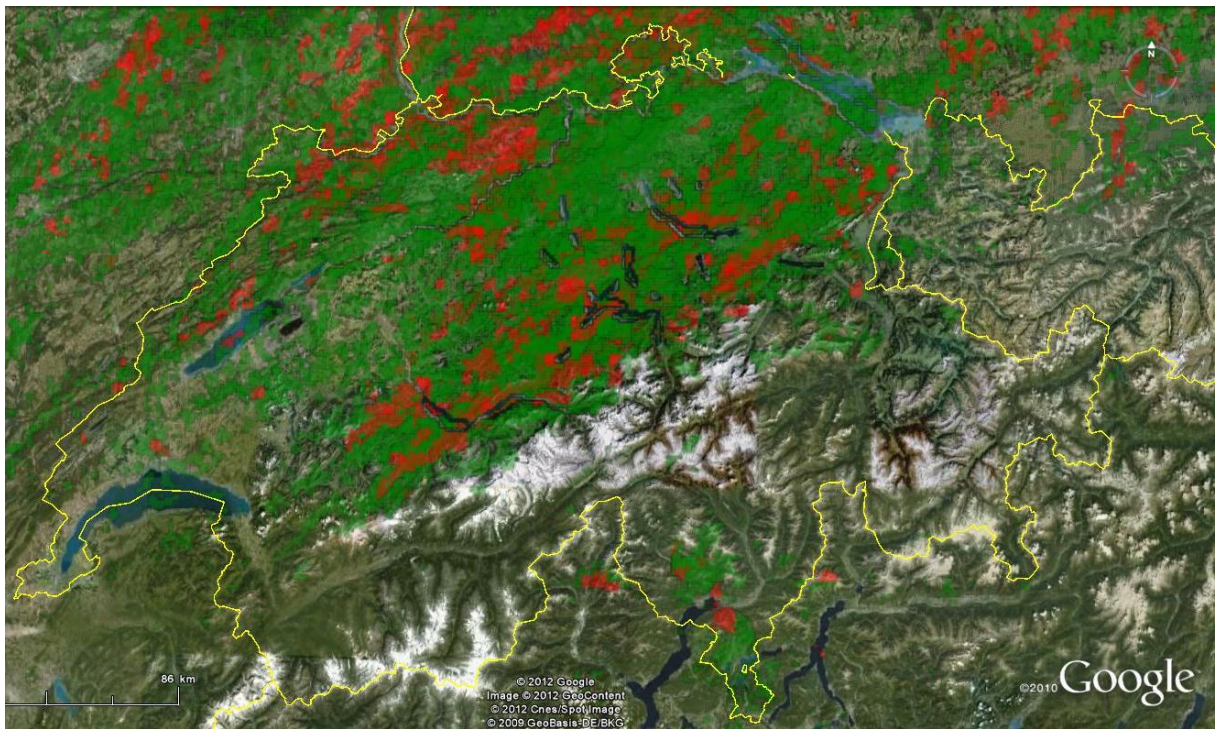


Figure 7.9: HAIL pixels of the hail season (May – September) 2011 in colors. The yellow lines are international borders.

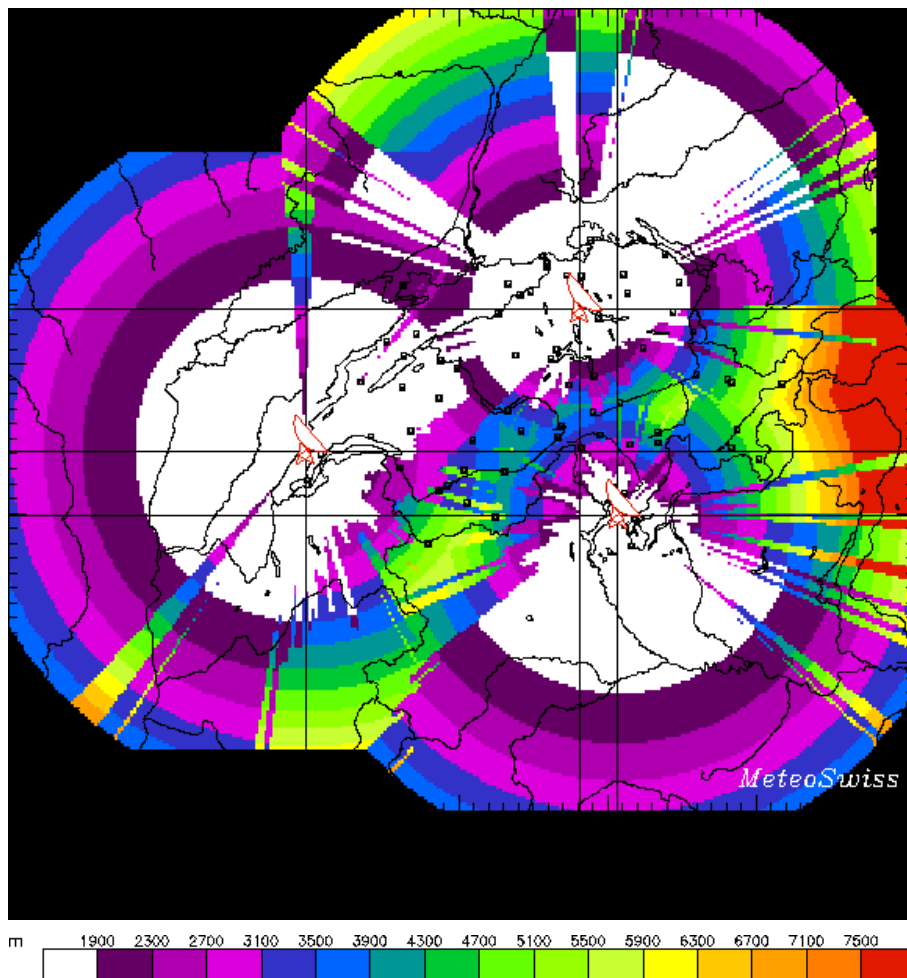


Figure 7.10: Visibility map of the Swiss radar composite with corresponding scale. White are regions with detection between 0-1900 m altitude. Red areas are regions where the height of detection is above 7500 m.

7.4. Examples of well captured small scale hail events

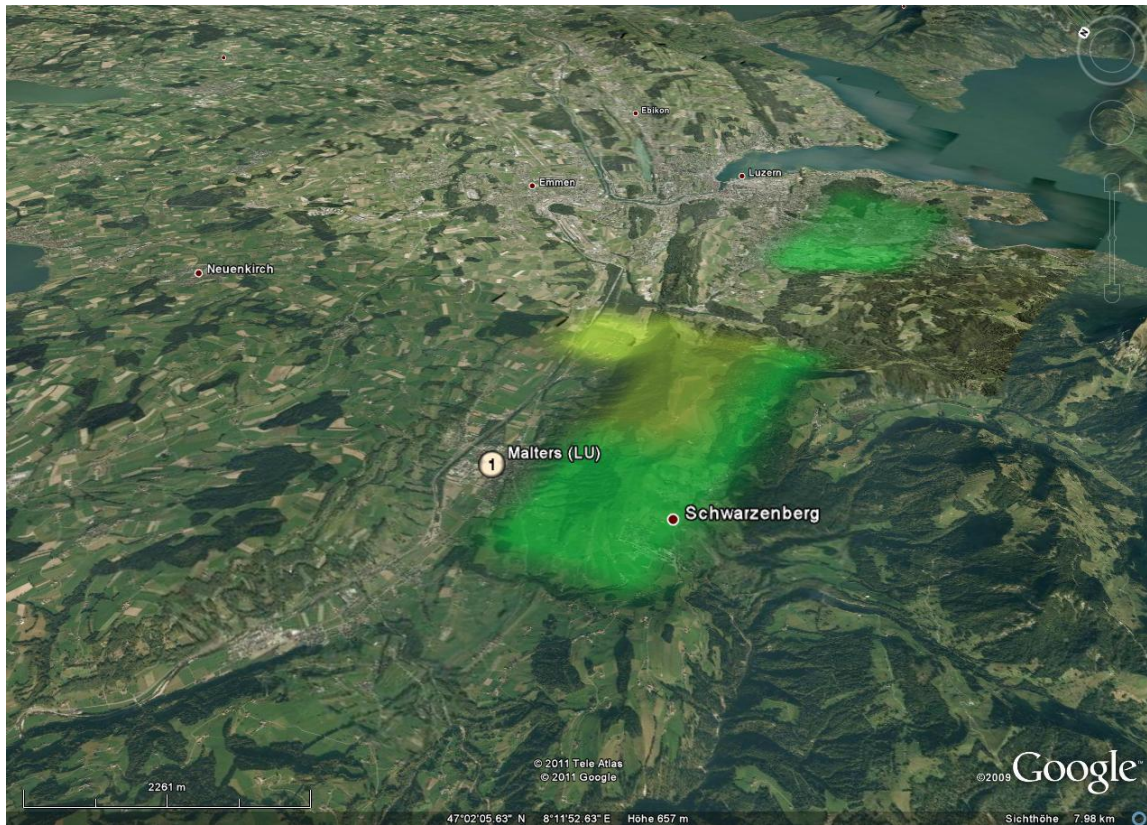


Figure 7.11: MESHS of May 05 2011 at the region of Malters (LU). The white point represents a ground-truth hail report of the commune Malters.

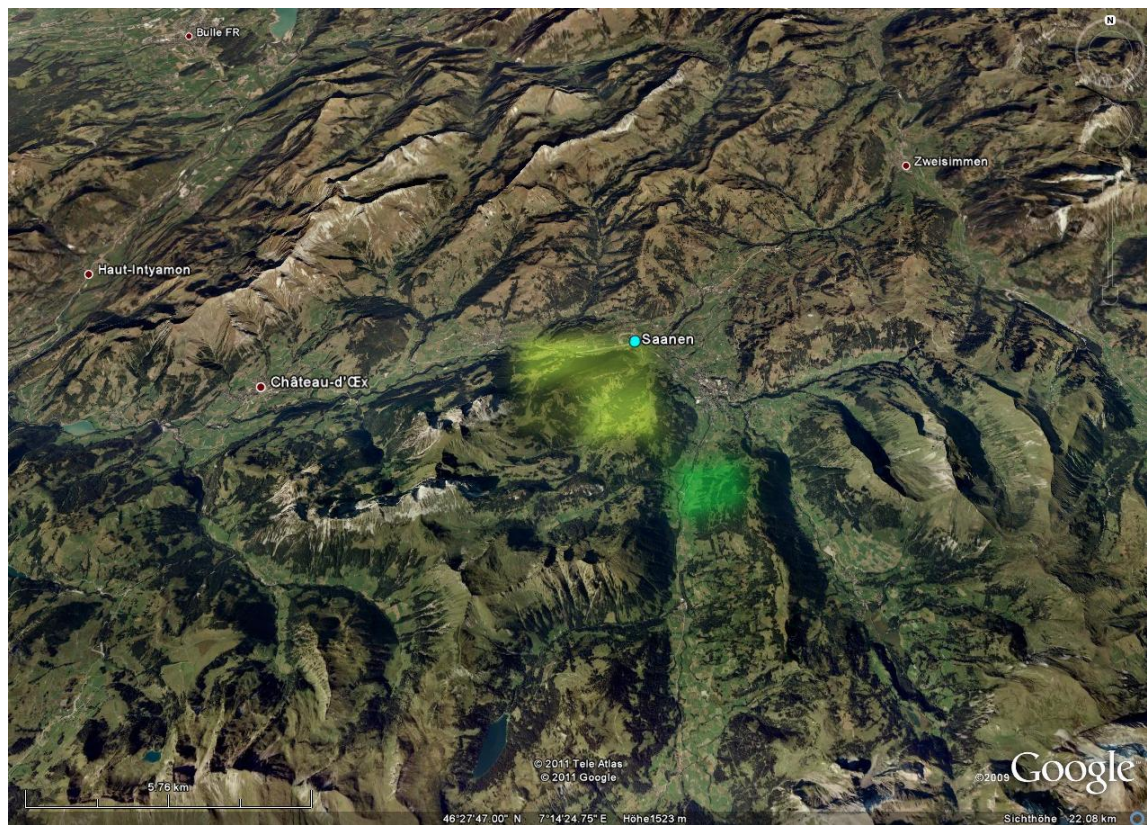


Figure 7.12: MESHS of June 29 2009 at the region of Gstaad/Saanen (BE). The blue-green point represents a ground-truth hail report of the commune Saanen.

8. References

- Brimelow, J.C., Reuter, G.W., Goodson, R., Krauss, T.W., (2006): Spatial Forecasts of Maximum Hail Size Using Prognostic Model Soundings and HAILCAST. *Weather and Forecasting*, 21: 206-219.
- Donaldson, R.J., Dyer, R.M., Kraus, M.J., (1975): An objective evaluator of techniques for predicting severe weather events. Preprints, 9th Conference on Severe Local Storms, Norman, OK, American Meteorological Society: 321-326.
- Ferree, J.T., Norman, O.K., Demuth, J., Eosco, G.M., Johnson, N.S., (2009): The increasing role of social media during high impact weather events. 37th Conference on Broadcast Meteorology.
- Germann, U., Galli, G., Boscacci, M. Bolliger, M., (2006), Radar precipitation measurement in a mountainous region. *Quarterly Journal of the Royal Meteorological Society*, 132: 1669–1692.
- Hering, A.M., Morel, C., Galli, G., Sényesi, S., Ambrosetti, P., Boscacci, M., (2004): Nowcasting thunderstorms in the Alpine region using a radar based adaptive thresholding scheme. Proc. ERAD Conference 2004, Visby, Sweden: 206-211.
- Hering, A.M., (2010): TRT (Thunderstorm Radar Tracking) documentation. MeteoSwiss, Locarno-Monti: 1-5.
- Holleman, I., (2001): Hail detection using single-polarization radar. Scientific Report, KNMI WR-2001-01: 1 – 72.
- Hyvärinen, O., Saltikoff, E., (2010): Social Media as a source of meteorological Observations. *American Meteorological Society*: 3175 – 3183.
- Hohl, R., Schiesser, H.H., Knepper, I., (2002): The use of weather radars to estimate hail damage to automobiles: an exploratory study in Switzerland. *Atmospheric Research*, 61: 215-238.
- Johns, R.H., Doswell, C.A., (1992): Severe local storms forecasting. *Weather and Forecasting*, 7: 588-612.
- Joss, J., Schädler, B., Galli, G., Cavalli, R., Boscacci, M., Held, E., Della Bruna, G., Kappenberger, G., Nespor, V., Spiess, R., (1997): Operational use of radar for precipitation measurements in Switzerland. MeteoSwiss, Locarno-Monti, 1999.
- Kessinger, C.J., Brandes, E.A., Smith, J.W., (1995): A comparison of the nexrad and nssl hail detection algorithms. 27th conference on Radar Meteorology, AMS, 603-605.
- OcCC, (2003): Extremereignisse und Klimaänderung: Wissensstand und Empfehlungen des OcCC. Bern: 65-68.
- Ortega, K.L., Smith, T.M., Scharfenberg, K.A., (2006): Analysis of thunderstorm hail fall patterns in the Severe Hail Verification Experiment. 23th Conference on Severe Local Storms, American Meteorological Society.
- Ortega, K.L., Smith, T.M., Stumpf, G., (2007): The severe hail verification experiment. 4th European Conference on Severe Storms, Italy.
- Ortega, K.L., Smith, T.M., Manross, K.L., Scharfenberg, K.A., Witt, A., Kolodziej, A.G., Gourley, J.J., (2009): The severe hazards analysis and verification experiment. BAMS, October 2009. American Meteorological Society: 1519-1530.
- Schiesser, H.H., Hohl, R., Schmid, W., (1998): Ueber die Beziehung Hagelfall – Gebäudeschäden: Fallstudie „Luzern-Hagelsturm“ vom 21. Juli 1998. Pilotstudie erstellt für die Partner Re. Institut für Atmosphärenphysik ETH-Hönggerberg.
- Schmid, W., Schiesser, H.H., Waldvogel, A., (1992): The kinetic energy of hailfalls. Part IV: Patterns of hailpad and radar data. *J. Appl.Meteor.*: 31, 1165-1178.

-
- Smith, T.M., Lakshmanan, V., (2006): Utilizing google earth as a gis platform for weather applications. 22th Conference on 25th Conference on International Interactive Information and Processing Systems (IIPS) for Meteorology, Oceanography, and Hydrology. American Meteorological Society.
- Stanley, A.C., (1970): Note on Hailstone size distributions. *Journal of Applied Meteorology*, 10: 168-170.
- Swiss Federal Statistical Office, (2011): Population: current state and change. Population density in 2000.
- Treolar, A.B.A, (1998). Vertically integrated radar reflectivity as an indicator of hail size in the greater sidney region of Australia. American Meteorological Society, 19th Conference on Severe Local Storms: 48-51.
- Waldvogel, A., Federer, B., Grimm, P., (1979). Criteria for the detection of hail cells. *Journal of Applied Meteorology*, 18: 1521-1525.
- Wilks, D.S., (1995): *Statistical Methods in the Atmospheric Sciences*. Academic Press, 467 pp.
- Willemse, S., (1995): A statistical analysis and climatological interpretation of hailstorms in Switzerland. Swiss Federal Institute of Technology (ETH), Diss. ETH No. 11137.
- Wilson, C.J., Ortega, K.L., Lakshmanan, V., (2009): Evaluating multi-radar, multi-sensor hail diagnosis with high resolution hail reports. 25th Conference on International Interactive Information and Processing Systems (IIPS) for Meteorology, Oceanography, and Hydrology. American Meteorological Society.
- Witt, A., (1990): A hail core aloft detection algorithm. Preprints, 16th Conference of Severe Local Storms and Conference Atmos. Electr., Kananaskis Park, American Meteorological Society, Boston: 232-235.
- Witt, A., Eilts, M.D., Stumpf, G.J., Johnson, J.T., Mitchell, E.D., Thomas, K.W., (1998): An enhanced hail detection algorithm for the wsr-88d. *Weather and Forecasting*, 13: 286-303.

Arbeitsberichte der MeteoSchweiz

- 237** Gehrig R: 2012, Die Repräsentativität der Pollenmessstationen des Schweizer Pollenmessnetzes, 76pp, CHF 77.-
- 236** Füllemann C, Begert M, Croci-Maspoli M and Brönnimann S: 2011, Digitalisieren und Homogenisieren von historischen Klimadaten des Swiss NBCN - Resultate aus DigiHom, 48pp, CHF 71.-
- 235** Weusthoff T: 2011, Weather Type Classification at MeteoSwiss - Introduction of new automatic classification schemes, 38pp, CHF 66.-
- 234** Hächler P, Burri K, Dürr B, Gutermann T, Neururer A, Richner H and Werner R: 2011, Der Föhnfall vom 8. Dezember 2006 – Eine Fallstudie, 47pp, CHF 68.-
- 233** Wüthrich C, Scherrer S, Begert M, Croci-Maspoli M, Marty C, Seiz G, Foppa N, Konzelmann T and Appenzeller C: 2010, Die langen Schneemessreihen der Schweiz - Eine basisklimatologische Netzanalyse und Bestimmung besonders wertvoller Stationen mit Messbeginn vor 1961, 33pp, CHF 64.-
- 232** Willi M: 2010, Gridding of Daily Sunshine Duration by Combination of Station and Satellite Data, 92pp, CHF 78.-
- 231** Scherrer S: 2010, Die Niederschlagstotalisatoren der Schweiz –Eine basisklimatologische Netzanalyse und Bestimmung besonders wertvoller Stationen, 32pp, CHF 64.-
- 230** Michel, D, MW Rotach, R Gehrig and R Vogt: 2010, Experimental investigation of micrometeorological influences on birch pollen emission, 37 pp, CHF 56. -
- 229** Philipona R, Levrat G, Romanens G, Jeannet P, Ruffieux D and Calpini B: 2009, Transition from VIZ / Sippicanto ROTRONIC - A new humidity sensor for the SWISS SRS 400 Radiosonde, 37pp, CHF 66.-
- 228** MeteoSchweiz: 2009, Klimabericht Kanton Graubünden, 40pp, nur als .pdf erhältlich
- 227** MeteoSchweiz, 2009, Basisanalysen ausgewählter klimatologischer Parameter am Standort KKWLeibstadt, 135pp, CHF 88.-
- 226** MeteoSchweiz: 2009, Basisanalysen ausgewählter klimatologischer Parameter am Standort KKW-Mühleberg, 135pp, CHF 88.-
- 225** MeteoSchweiz: 2009, Basisanalysen ausgewählter klimatologischer Parameter am Standort KKW-Gösgen, 135pp, CHF 88.-
- 224** MeteoSchweiz: 2009, Basisanalysen ausgewählter klimatologischer Parameter am Standort KKW-Beznau, 135pp, CHF 88.-
- 223** Dürr B: 2008, Automatisiertes Verfahren zur Bestimmung von Föhn in den Alpentälern, 22pp, CHF 62.-
- 222** Schmutz C, Arpagaus M, Clementi L, Frei C, Fukutome S, Germann U, Liniger M and Schacher F: 2008, Meteorologische Ereignisanalyse des Hochwassers 8. bis 9. August 2007, 29pp, CHF 64.-
- 221** Frei C, Germann U, Fukutome S and Liniger M: 2008, Möglichkeiten und Grenzen der Niederschlagsanalysen zum Hochwasser 2005, 19pp, CHF 62.-
- 220** Ambühl J: 2008, Optimization of Warning Systems based on Economic Criteria, 79pp, CHF 75.-
- 219** Ceppi P, Della-Marta PM and Appenzeller C: 2008, Extreme Value Analysis of Wind Observations over Switzerland, 43pp, CHF 67.-
- 218** MeteoSchweiz (Hrsg): 2008, Klimaszenarien für die Schweiz – Ein Statusbericht, 50pp, CHF 69.-

Veröffentlichungen der MeteoSchweiz

- 88** Schibli R: 2011, Spatio-temporal homogeneity of a satellite-derived global radiation climatology, 110pp, CHF 82.-
- 87** Bischof M: 2011, Ensemble Simulations of Convective Storms, 120pp, CHF 84.-
- 86** Walker, D: 2010, 2010, Cloud effects on erythemal UV radiation in a complex topography, 106 pp, CHF 81.-
- 85** Ambühl J: 2010, Neural interpretation of ECMWF ensemble predictions, 48pp, CHF 68.-
- 84** Ambühl J: 2010, Customer oriented warning systems, 91pp, CHF 78.-
- 83** Ceppi P: 2010, Spatial characteristics of gridded Swiss temperature trends: local and large-scale influences, 82pp, CHF 76.-
- 82** Blanc P: 2009, Ensemble-based uncertainty prediction for deterministic 2 m temperature forecasts, 90pp, CHF 78.-
- 81** Erdin R: 2009, Combining rain gauge and radar measurements of a heavy precipitation event over Switzerland: Comparison of geostatistical methods and investigation of important influencing factors, 109pp, CHF 81.-
- 80** Buzzi M: 2008, Challenges in Operational Numerical Weather Prediction at High Resolution in Complex Terrain, 186pp, CHF 103.-
- 79** Nowak D: 2008, Radiation and clouds: observations and model calculations for Payerne BSRN site, 101 pp, CHF 80.-
- 78** Arpagaus M, Rotach M, Ambrosetti P, Ament F, Appenzeller C, Bauer H-S, Bouttier F, Buzzi A, Corazza M, Davolio S, Denhard M, Dorninger M, Fontannaz L, Frick J, Fundel F, Germann U, Gorgas T, Grossi G, Hegg C, Hering A, Jaun S, Keil C, Liniger M, Marsigli C, McTaggart-Cowan R, Montani A, Mylne K, Ranzi R, Richard E, Rossa A, Santos-Muñoz D, Schär C, Seity Y, Staudinger M, Stoll M, Vogt S, Volkert H, Walser A, Wang Y, Werhahn J, Wulfmeyer V, Wunram C and Zappa M: 2009, MAP D-PHASE: Demonstrating forecast capabilities for flood events in the Alpine region. Report of the WWRP Forecast Demonstration Project D-PHASE submitted to the WWRP Scientific Steering Committee, 65pp, CHF 73.-
- 77** Rossa AM: 2007, MAP-NWS – an Optional EUMETNET Programme in Support of an Optimal Research Programme, 67pp, CHF 73.-
- 76** Baggensto D: 2007, Probabilistic verification of operational monthly temperature forecasts, 52pp, CHF 69.-
- 75** Fikke S, Ronsten G, Heimo A, Kunz S, Ostrozlik M, Persson PE, Sabata J, Wareing B, Wichura B, Chum J, Laakso T, Säntti K and Makkonen L: 2007, COST 727: Atmospheric Icing on Structures Measurements and data collection on icing: State of the Art, 110pp, CHF 83.-
- 74** Schmutz C, Müller P and Barodte B: 2006, Potenzialabklärung für Public Private Partnership (PPP) bei MeteoSchweiz und armasuisse Immobilien, 82pp, CHF 76.-
- 73** Scherrer SC: 2006, Interannual climate variability in the European and Alpine region, 132pp, CHF 86.-
- 72** Mathis H: 2005, Impact of Realistic Greenhouse Gas Forcing on Seasonal Forecast Performance, 80pp, CHF 75.-
- 71** Leuenberger D: 2005, High-Resolution Radar Rainfall Assimilation: Exploratory Studies with Latent Heat Nudging, 103pp, CHF 81.-
- 70** Müller G und Viatte P: 2005, The Swiss Contribution to the Global Atmosphere Watch Programme – Achievements of the First Decade and Future Prospects, 112pp, CHF 83.-
- 69** Müller WA: 2004, Analysis and Prediction of the European Winter Climate, 115pp, CHF 34.